Composite Structures 298 (2022) 115998

Contents lists available at ScienceDirect

Composite Structures

journal homepage: www.elsevier.com/locate/compstruct

A hybrid numerical-experimental strategy for predicting mechanical response of components manufactured via FFF

Narges Dialami [a,*], Michele Chiumenti [a], Miguel Cervera [a], Uxue Chasco [a], Guillermo Reyes-Pozo [b], Marco A. Pérez [b]

[a] International Center for Numerical Methods in Engineering (CIMNE), Universidad Politécnica de Cataluña, Campus Norte UPC, 08034 Barcelona, Spain
[b] IQS School of Engineering, Universitat Ramon Llull, Via Augusta 390, 08017 Barcelona, Spain

ARTICLE INFO

Keywords:
Material characterization
Fused Filament Fabrication
Mechanical properties
Anisotropy
Hybrid methodology

ABSTRACT

In this paper a new methodology developed for predicting the mechanical performance of the structures additively manufactured by Fused Filament Fabrication is presented.

The novelty of the approach consists in accounting for the anisotropy in the material properties induced by the printing patterns. To do so we partition the manufactured structure according to the printing patterns used in a single component. For determining the material properties of each partition, a hybrid experimental/computational characterization is proposed.

The external partitions with aligned (contour) and crossed (cover) filaments are characterized through uniaxial tensile tests on General Purpose Acrylonitrile Butadiene Styrene dog-bone samples with corresponding patterns. Characterization of the inner structure (infill/lattice) is done through computational homogenization technique using Representative Volume Element.

The presented methodology is validated against experimental results of square cross-section demonstrators. It is shown that the material properties depend on the geometrical relationship of the different printing patterns, exclusively. Therefore, the exhaustive experimental procedure can be avoided characterizing the printed material by a pre-defined anisotropic constitutive relationship proportional to the properties of the raw material. Moreover, the acquired geometrical relationship is validated for components made of Polylactic Acid.

The given methodology may be used as design-for-manufacture tool for creating functional components.

1. Introduction

In recent years new manufacturing technologies have been developed seeking to optimize various aspects of the finished product: material and energy costs, ease of manufacturing and mechanical performance. One of the most outstanding technologies is Additive Manufacturing (AM), also called "3D printing", which consists in the progressive (layer-by-layer) addition and adhesion of material to manufacture the final product on the basis of a 3D CAD model.

The emergence of this technology traces back to the 1980 s, when the first three printing techniques were patented: stereolithography (SLA), selective laser sintering (SLS), and fused deposition modelling (FDM). These techniques were intended to quickly create 3D prototypes using exclusively polymeric materials (Ligon et al, 2018 [1]). Currently, there are more 3D printing techniques, and a wider range of materials is accessible, ranging from metals to biomaterials (Pîrjan & Petroşanu, 2013 [2]). Owing to this, AM is used in countless applications, including medicine, art, fashion, military, architecture, engineering, education, jewellery, computing, automotive, aeronautics and even in construction, gastronomy and aerospace (Dormehl, 2018 [3]).

The present work focuses on one of the first AM techniques, well established for polymeric materials: FDM, also called Fused Filament Fabrication (FFF) (Brenken et al., 2018 [4]). Of all the AM techniques available today, FFF is the best known and the most widely used due to its versatility and suitability for operating with a wide range of materials.

FFF is based on the extrusion of the printing material through a nozzle to reproduce a 3D CAD model. The deposition process is carried out by melting the filaments of a certain thermoplastic material. The extruded material is deposited layer by layer on a printing table. Simultaneous movements of the nozzle and the printing table allow the

* Corresponding author.
E-mail addresses: Narges.Dialami@upc.edu (N. Dialami), Michele.Chiumenti@upc.edu (M. Chiumenti), Miguel.Cervera@upc.edu (M. Cervera), Uxuech9@gmail.com (U. Chasco), Guillermo.Reyes@iqs.url.edu (G. Reyes-Pozo), Marcoantonio.Perez@iqs.url.edu (M.A. Pérez).

https://doi.org/10.1016/j.compstruct.2022.115998
Received 26 December 2021; Received in revised form 27 May 2022; Accepted 22 July 2022
Available online 25 July 2022

Nomenclature

E	Young's modulus
G	Shear modulus
ν	Poisson's ratio
Raw	Raw material
σ_M	Average stress
ε_M	Average strain
$\mathbf{C}$	Stiffness tensor
$\mathbf{S}$	Compliance matrix
iso	Plane of isotropy
$\perp$	Direction perpendicular to the plane of isotropy
$\|\|$	Direction parallel to the filament
$\mathbf{X}$	Coordinate at macro scale
$\mathbf{x}$	Coordinate at micro scale
$\mathbf{u}$	Displacement field
$\boldsymbol{\varepsilon}$	Strain field
$\boldsymbol{\sigma}$	Stress field
m	Macro scale
μ	Micro scale
$\sim$	Fine scale contribution
V_{RVE}	RVE volume
Γ_{RVE}	RVE boundary
$\mathbf{t}$	Tractions
$\nabla^S(\bullet)$	Symmetric part of gradient
ε_{rel}	Relative error
K	Stiffness
r	Residual error
S	Objective function

deposition in 3D, thus enabling the system to manufacture complex 3D geometries.

Another attractive feature of FFF consists in the fact that it allows modifying the material properties by designing the microstructure of a component. The material properties of the resulting printed component can differ from the ones of the crude material (Kotlinski, 2014 [5]). In spite of the isotropic behaviour of the raw material, the final behaviour of the FFF built components are anisotropic. The anisotropic material behaviour is the result of layer-to-layer and filament-to-filament adhesions in addition to the printing patterns (Khudiakova et al, 2019 [6]). Moreover, intrinsic defects such as voids present in the FFF printed components also lead to anisotropic mechanical properties [7]. The inter-bead voids are generally consistent in shape, orientation and distribution. The intra-bead voids are inherent to FFF components of composite materials. Voids filled and unfilled with the resin in the middle of filaments are trapped by the folding of the overflow material in the moulded filaments resulting in an asymmetric section [8]. If voids exceed a certain volume (typically 5–6 %), this implying unfilled resin in the laminate (typically 10–12 %), void orientation may lead to errors in the estimation of the void measurements using image analysis [9].

The printing procedure and, thus, the final characteristic of the component are controlled by various process parameters. The most significant ones are the component orientation, the layer thickness and the pattern designs. These parameters are selected prior to printing and affect the mechanical performance of the components (Li et al, 2018 [10]). Therefore, performance analysis of FFF built components is an exigence from the AM users.

Ding et al. [11] studied the effect of nozzle temperature, building orientation and material properties on the morphology and chemical composition of Poly-ether-ether-ketone (PEEK) and polyetherimide (PEI) printed materials.

Chacon et al. [12] investigated the effect of build orientation, layer thickness and feed rate on the mechanical performance of PLA samples for optimal settings and the mechanical behaviour of 3D printed components.

Zou et al. [13] studied the effect of printing orientation on the mechanical property of acrylonitrile butadiene styrene (ABS) samples. Isotropic and transversely isotropic elasticity constitutive models were used to define the relation of elastic constants and printing angles.

Garzon-Hernandez et al. [14] investigated the influence of layer height, number of layers and raster orientation on the mechanical response of the ABS samples. A constitutive model was developed considering the nonlinear behaviour, strain rate in both elastic and.

inelastic regimes and transverse isotropy behaviour.

Considering the printing pattern, a FFF structure is characterized by three zones: the contour, that is made of aligned filaments, the inner structure, that is in-fill or lattice type, and the top and bottom covers,

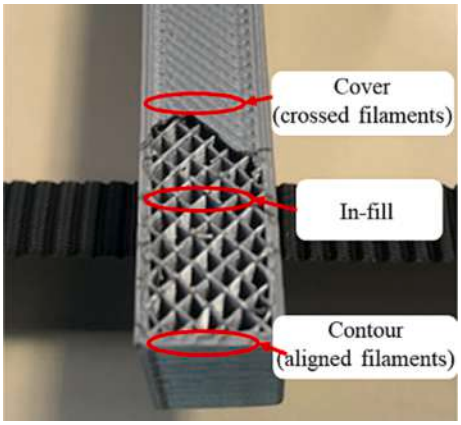

Fig. 1. Different zones of a FFF component.

that are made of filaments with full density (100 %) crossed pattern and 45 ° raster angle (Fig. 1). The contour includes most of the external surfaces where the slope relative to the printing plane is greater than 30°. The covers are top and bottom surfaces with the slope below 30°.

In the inner part, the in-fill is the standard structure with density defined through the raster to raster air gap, while the lattice structure is characterized by periodically repeated unit cells. These types of inner structures are for reducing the amount of material, cost and time of production which make the FFF technique advantageous over the rest of AM technologies (Aloyaydi et al, 2019 [15]).

Numerous experimental studies have corroborated that products made by FFF have anisotropic mechanical performance, i.e., the mechanical properties depend on the direction in which they are manufactured (Ahn et al., 2002 [16]; Somireddy and Czekanski, 2017 [17]; Zou et al., 2016 [13]; Dizon et al., 2018 [18]; Popescu et al., 2018 [19]; Gabor et al., 2019 [20]). Likewise, in various research works, the stress–strain curves resulting from experimental tests of specimens manufactured using FFF have been obtained (Domingo-Espin et al., 2015 [21]; Casavola et al., 2016 [22]). These graphs show the regions of linear and non-linear behaviour, which indicate presence of elastic and plastic deformations. They found that, on the one hand, the resistance of the adhering layers in built direction (typically Z direction) is weaker compared to other directions; on the other hand, the resistance of material is greater in a direction parallel to the filament threads deposited in the same layer (Domingo-Espin et al., 2015 [21]). The described behaviour is highly dependent on the printing parameters (Rodríguez et al., 2001 [23]). The obtained results in the previous work of the authors [24] indicate that both the intra-layer and the inter- layer bonds

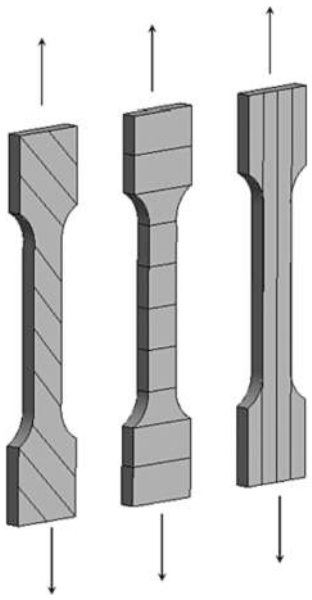

Fig. 2. Different building orientations of a test specimen manufactured by FFF.

play a significant role in the behaviour of the FFF samples. In this sense, the use of the thermal chamber reduces the temperature gradient between the deposited filament and the last layer built. This fact strengthens the unions, improves mechanical performance, and decreases the degree of orthotropy. Furthermore, the results obtained confirm that the stiffness on the direction of the extruded filament is higher than the one of the intra-layer unions between contiguous filaments. However, the rigidity of the inter-layer cohesion of adjacent layers is the lowest. Fig. 2 illustrates 3 geometrically identical samples, but printed in 3 different orientations, subjected to identical stretching. Even though the global stresses are the same in all the three cases, the state of the stresses is different in the material axes of each specimen. Due to the filament orientation, the sample on the right hand side has the highest strength along the tensile axis.

Even though various experimental investigations revealed the effect of the printing patterns on the properties of the printed parts, there exist only a few works dealing with the analytical and computational assessment of the mechanical performance of FFF components. Casavola et al [22] identified the orthotropic properties of the FFF components made of acrylonitrile butadiene styrene (ABS) and polylactic acid (PLA) by Classical Lamination Theory (CLT). Garg and Bhattacharya [25] modelled the deformation of the FFF components under uniaxial force using diversity of raster thicknesses and printing orientations. The existing works use a single solid model for the characterization of the material. However, the structural response of contour, cover and inner structures is different according to the manufacturing pattern and the infill density. The contour is stiffer along the axis of the printing plane parallel to the filaments. The cover behaves isotropically on the printing plane due to the symmetry of the pattern.

Generally, FFF printed parts include a zone surrounding the entire component with filaments aligned (contour), a zone at top and bottom of the entire structure with crossed filaments (cover) and the infill zone where the printing pattern changes case to case.

In this work, a novel methodology for the analysis of the mechanical performance of FFF built components that takes into account the different mechanical properties of the contour, the cover and the inner structure is developed. Material properties of each part is identified experimentally and computationally (section 2).

First, the geometry is divided into different volumes according to the printing patterns. Extensive experimental tests are performed to evaluate the anisotropic properties of the contour and the cover. The characterized material, ELIX ABS-3D GP, developed by Elix Polymers, is a precolored or natural General Purpose Acrylonitrile Butadiene Styrene (ABS) grade. It presents enhanced printing performance, low warpage, dimensional exactness and high resolution. ELIX ABS-3D GP is intended for use in FFF in 3D printing applications. ABS-3D GP Dog-bone samples are manufactured exclusively with aligned and crossed filaments to represent the contour and the cover, respectively. The samples are tested uniaxially at different orientations. Anisotropic linear elastic constitutive models are considered to describe the mechanical behaviour of contour, cover and in-fill. A geometrical relationship is found between the material parameters at different orientation and the raw material. The characterization of the infill is done computationally by the homogenization method. The constitutive matrix of the inner structure is modelled using computational homogenization technique by Representative Volume Element (RVE).

This division considers 3 different materials in a single component as the printing patterns affect both the material properties and behaviour.

An experimental campaign for the validation of the developed computational model differentiating the mechanical behaviour of the contour, the cover and the in-fill and defining their respective material properties through experimental characterization is set up (section 3). For this purpose, ABS-3D GP samples with square cross-section subjected to bending load are built and tested.

Next, an experimental campaign on the door-handle components is set up in order to analyse the mechanical performance of FFF objects

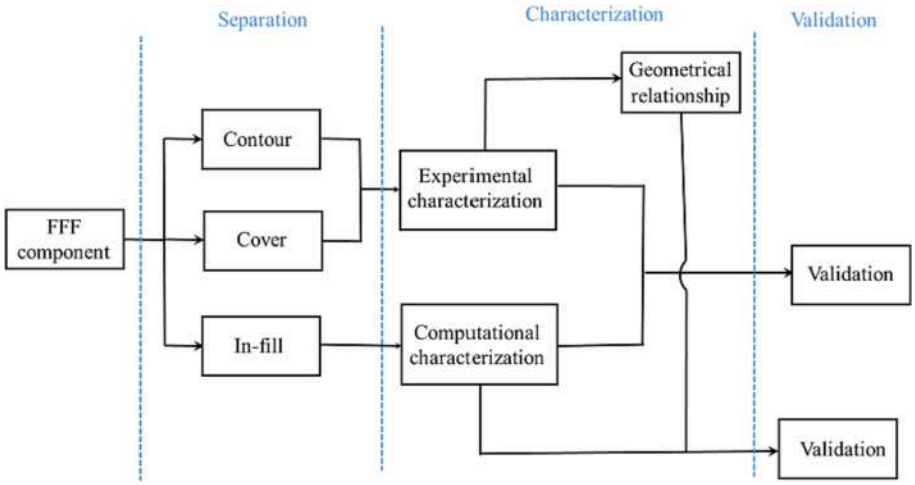

Fig. 3. The strategy for the material characterization.

W – Width of narrow section: 13 mm
L – Length of narrow section: 57 mm
WO – Width overall: 19 mm
LO – Length overall: 165 mm
G – Gage length: 50 mm
D – Distance between grips: 115 mm
R – Radius of fillet: 76 mm
T – Thickness: 7 mm

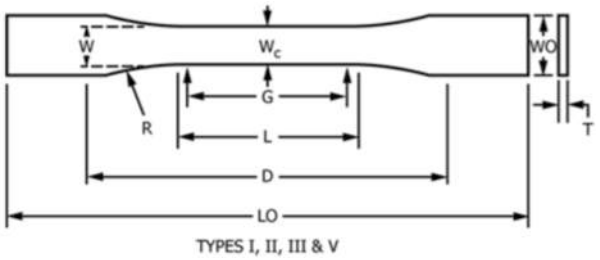

Fig. 4. Dog-bone specimen dimension (ASTM D638).

(section 4). The acquired relationship is considered for characterization of the PLA filaments according to the printing pattern. The computational model and the established geometrical relationship between the material parameters are validated using PLA door-handle components subjected to bending and torsion loading. In this case, the effect of the printing orientation and process parameters on the final structural performance is explored.

The model proposed in this work can be used as a design-for-manufacture (DFAM) approach in order to create functional components.

2. Methodology: Hybrid experimental and computational material characterization

In this section, the hybrid methodology for the performance analysis of the components built by FFF technology are presented (see Fig. 3). The methodology consists of both experimental and computational characterization.

As mentioned, a component built by FFF technology includes three distinct zones according to their printing pattern and orientation revealing different mechanical behaviour. These zones are the contour, the cover and the inner structure (in-fill). The contour is made of aligned filaments with the external edges of the FFF components while the cover is made of crossed filaments with rectilinear pattern. The inner structure (in-fill) is made of raster with a certain density that is the raster to raster space.

The mechanical properties of the printed material are different from those of the raw material. The contour, the cover and the in-fill are anisotropic while the raw material is isotropic. Moreover, according to the printing pattern, the anisotropic properties differ. The printing pattern has a significant role on the material characterization and the orientation of both the isotropic plane and the weakest direction. In case of the cover and the in-fill, the printing plane is isotropic due to the symmetry of the pattern. The anisotropy develops in the build direction. In case of the contour, the stiffness in the filament direction (which is the anisotropic direction) is higher than the one of the intra-layer unions between filaments.

In this work, the anisotropic material properties of the ABS-3D GP made contour and cover are identified through experimental tensile tests on samples printed with the corresponding patterns. As the material properties are associated to the printing pattern, a geometrical relationship between the mechanical parameters at different orientations is found. Moreover, the mechanical properties of the printed material as a function of the raw material properties are determined. The obtained relationship can be used for characterizing materials used in FFF, avoiding an exhaustive experimental campaign.

Standard FE analysis of FFF components with in-fill or lattice inner structures is challenging due to the complexity of the mesh generation appropriate for such complex geometries. The inner structure is heterogeneous, thus its discretization by the standard FE mesh leads to an exaggerated element number, and therefore the numerical computations become unfeasible. The computational homogenization technique represents the corresponding anisotropic behaviour using an equivalent homogeneous continuum profiting from its repetitive cell structure. In this manner, the heterogeneities of the inner structure are not straightforwardly embedded into the structural analysis yet modelled through defining a RVE.

Even though the inner structure is characterized computationally, the input data for the homogenization technique is fed from the experimental characterization of the aligned filaments of the contour.

Overall, this work distinguishes between the mechanical behaviour of the contour, the cover and the in-fill. Thus, their respective mechanical properties are determined separately. However, separate experimental tests for the characterization of the contour, the cover and the in-fill may be challenging. Alternatively, the numerical model can be calibrated by a sensitivity analysis based on the raw material properties.

Table 1
Raw material properties.

ABS GP	
E_{Raw}	ν_{Raw}
Young's modulus (MPa)	Poisson's ratio
2230	0.34

2.1. Experimental tensile test on dog-bone samples

This section describes the experimental material characterization to determine the material constitutive tensor for the contour and the cover of FFF components.

The tensile test is performed in accordance with the ASTM D638 standard Test Method for Tensile Properties of Plastics. Twenty-four dog-bone samples of ELIX ABS-3D GP material are manufactured by FFF with different printing orientations (P-Z, P-ZX, P-ZY, P-H, I-Z, I-ZX, I-ZY and I-H) following the printing patterns used for contour and cover (see section 2.1.1). Standard specimen type I is chosen for the performance of these tests. The dimension of each specimen is shown in Fig. 4. From the tensile test results, Young's and shear moduli are obtained.

The isotropic elastic properties of the pre-printed material are shown in Table 1 [26,27].

To evaluate deformations in a 3D space, two Allied Vision GigE MAKO G-507B cameras together with a GOM Digital Image Correlation (DIC) software are used. DIC is an effective experimental technique to measure displacements and strains by comparing the images of the specimen covered with speckles before and after deformation. This procedure also allows measuring Poisson's coefficient. The results from the calibration of the DIC equipment, as well as the contactless extensometer definition criteria, can be seen in Fig. 5. Poisson's ratio of each tested sample is calculated via a DIC setup.

Thus, Poisson's ratio can be calculated (Table 2) on both front (ν_{21}) and side (ν_{31}) surfaces as:

$$\nu_{21} = \frac{\text{Facet Point 3} \leftrightarrow \text{Facet Point 4}}{\text{Facet Point 2} \leftrightarrow \text{Facet Point 1}}, \nu_{31} = \frac{\text{Facet Point 7} \leftrightarrow \text{Facet Point 8}}{\text{Facet Point 5} \leftrightarrow \text{Facet Point 6}} \quad (1)$$

A rate of 5 ± 25 % mm/min is selected for the tensile test according to Specimen Type I for rigid and semirigid samples.

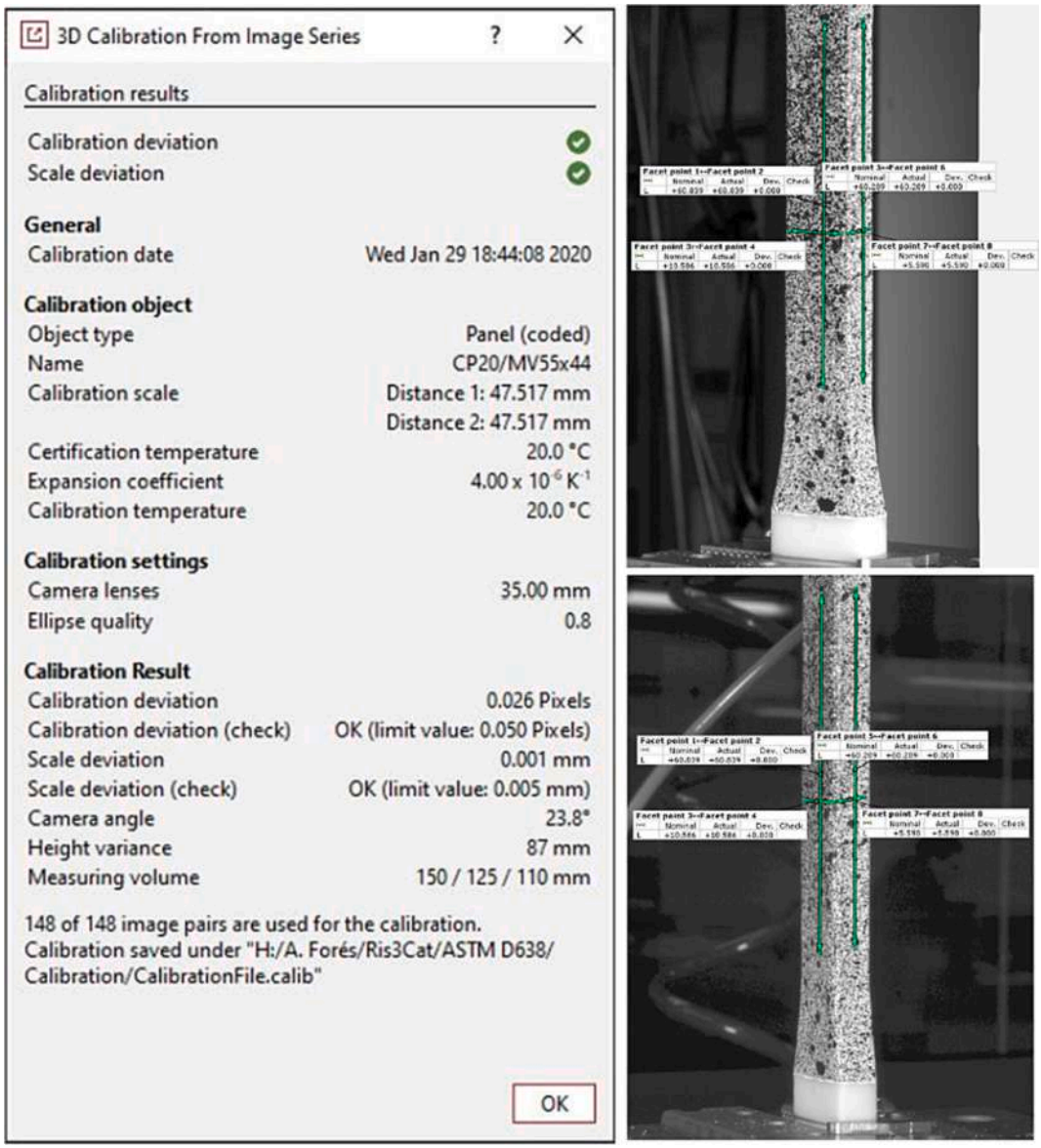

Fig. 5. DIC equipment calibration results (left) and contactless extensometer definition criteria (centre & right).

Table 2
Poisson's coefficient: DIC results.

	1-ν_{21}	2-ν_{21}	3-ν_{21}	Avg.	1-ν_{31}	2-ν_{31}	3-ν_{31}	Avg.
P-Z	0.253	0.333	0.245	**0.277** ± 0.049	0.359	0.373	0.167	**0.300** ± 0.115
P-ZX	0.443	0.419	0.317	**0.393** ± 0.067	0.571	0.366	0.319	**0.419** ± 0.134
P-ZY	0.337	0.295	0.426	**0.353** ± 0.067	0.293	–	–	**0.293** -
P-H	0.239	0.366	0.292	**0.299** ± 0.064	–	0.379	0.282	**0.331** ± 0.069
I-Z	–	–	–	–	–	–	–	–
I-ZX	0.086	0.246	0.232	**0.188** ± 0.088	0.504	–	0.208	**0.356** ± 0.210
I-ZY	0.249	0.161	0.240	**0.217** ± 0.048	–	0.513	–	**0.513** ± 0.296
I-H	0.327	0.367	0.295	**0.330** ± 0.036	0.346	0.281	–	**0.314** ± 0.184

The yield point has been identified following the offset method for determining yield strength with an offset value of 0.1 %. The tensile stress–strain data obtained for each specimen tested is presented in Table 3. The stiffness, maximum load and material failure vary depending on the printing pattern, orientation and testing direction.

Fig. 6 demonstrates the load–displacement relationship in each testing configuration.

2.1.1. Material characterization of the contour and cover

The nomenclature used for the specimens corresponds to contour (P) and cover (I). Fig. 7 shows the printing position of each specimen with respect to the reference axes. In the case of contour (P), the filament pattern follows the extrusion machine, parallel to one of the axes of the construction plane. In the case of cover (I), the printing pattern of the filament is crossed with 45° raster angle placed in the construction plane. The printing design and the printed specimens at different

Table 3
Average stress and average strain: Tensile test on dog-bone specimens.

#	Orient.	σ_M MPa		ε_M %		#	Orient.	σ_M MPa		ε_M %	
1	P-Z	14.9	15.4 ± 1.4	1.04	1.14 ± 0.13	13	I-Z	2.1	2.3 ± 0.5	0.17	0.15 ± 0.05
				1.06						0.16	
2	P-Z	17.0		1.30		14	I-Z	2.8		0.21	
				1.32						0.15	
3	P-Z	14.3		1.06		15	I-Z	2.1		0.10	
				1.05						0.08	
4	P-ZX	15.7	19.0 ± 3.0	0.95	1.38 ± 0.34	16	I-ZX	7.7	9.8 ± 4.4	0.76	1.79 ± 1.62
				0.98						0.66	
5	P-ZX	21.4		1.72		17	I-ZX	14.9		3.88	
				1.70						3.87	
6	P-ZX	20.0		1.48		18	I-ZX	6.8		0.80	
				1.48						0.76	
7	P-ZY	10.2	11.0 ± 1.8	0.69	0.73 ± 0.13	19	I-ZY	7.7	7.0 ± 0.8	0.81	0.83 ± 0.07
				0.68						0.87	
8	P-ZY	13.1		0.87		20	I-ZY	7.3		0.88	
				0.92						0.91	
9	P-ZY	9.7		0.61		21	I-ZY	6.1		0.73	
				0.62						0.79	
10	P-H	31.3	28.9 ± 2.3	2.76	1.90 ± 0.67	22	I-H	18.2	19.7 ± 2.0	1.96	1.85 ± 0.14
				2.75						1.99	
11	P-H	28.7		1.58		23	I-H	18.9		1.66	
				1.53						1.71	
12	P-H	26.7		1.38		24	I-H	22.0		1.83	
				1.37						1.93	

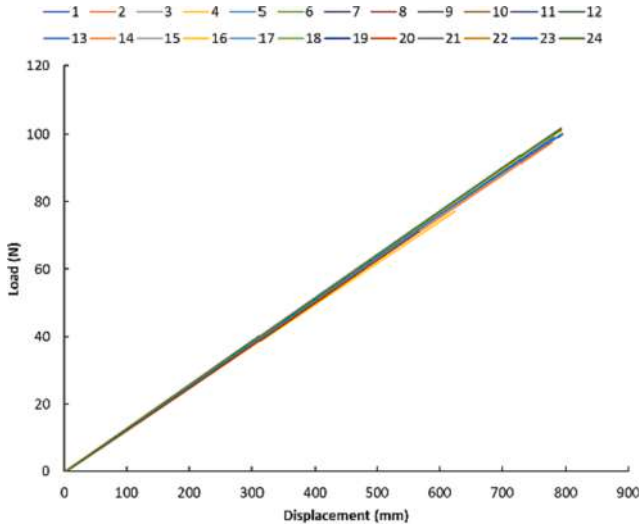

Fig. 6. Load-displacement relationship in each testing configuration.

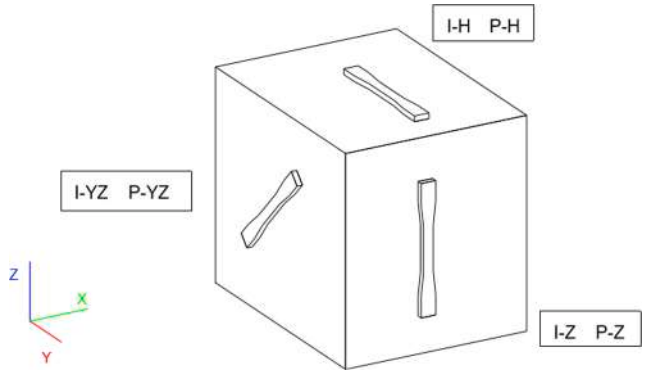

Fig. 7. Orientations of the dog-bone specimens with respect to the reference axes.

orientations are shown in Figs. 8 and 9.

The nomenclature, H, Z, YZ and XZ corresponds to the following.

- H: The sample is printed in the XY plane and placed horizontally (H).
- Z: The sample is printed in the XY plane and placed vertically (Z) on the plane aligned with the Z direction.
- YZ: The sample is printed with 45° degrees of inclination in YZ plane.
- XZ: The sample is printed with 45° degrees of inclination in XZ plane (similar to the YZ case).

According to the constitutive equation of a linear elastic material, the stiffness tensor **C** has to be obtained from the experiment. The inverse of the constitutive tensor is known as the compliance matrix$\mathbf{S} = \mathbf{C}^{-1}$. The experimental tests are defined such that to obtain the transversely isotropic material properties.

Since the model is constructed layer by layer during the FFF process, the material properties can be considered transversely isotropic: the mechanical properties are symmetric in all directions of the transverse plane normal to an anisotropic principal axis along the direction of deposition.

Due to this symmetry presented in 2D, the material properties are reduced from 9 (orthotropic materials) to 5 independent parameters (transversely isotropic material).

In order to obtain the 5 independent material parameters, samples are built with 3 different orientations: horizontal, vertical and 45° inclined.

The cover and the contour material are assumed to be transversely isotropic. According to the reference axes used in the experiment, the following nomenclature is defined for each zone.

Contour:

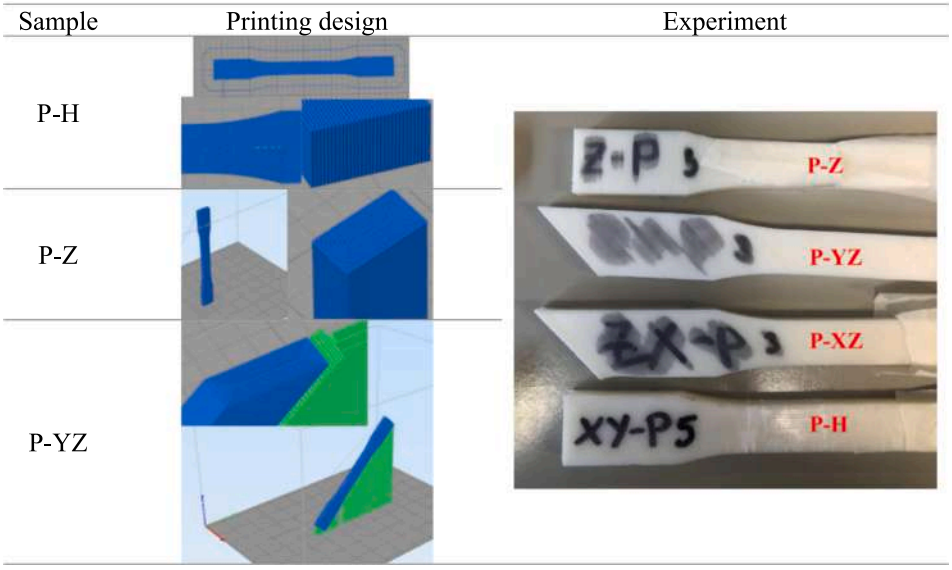

Fig. 8. P samples (contour): Printing design and printed specimen.

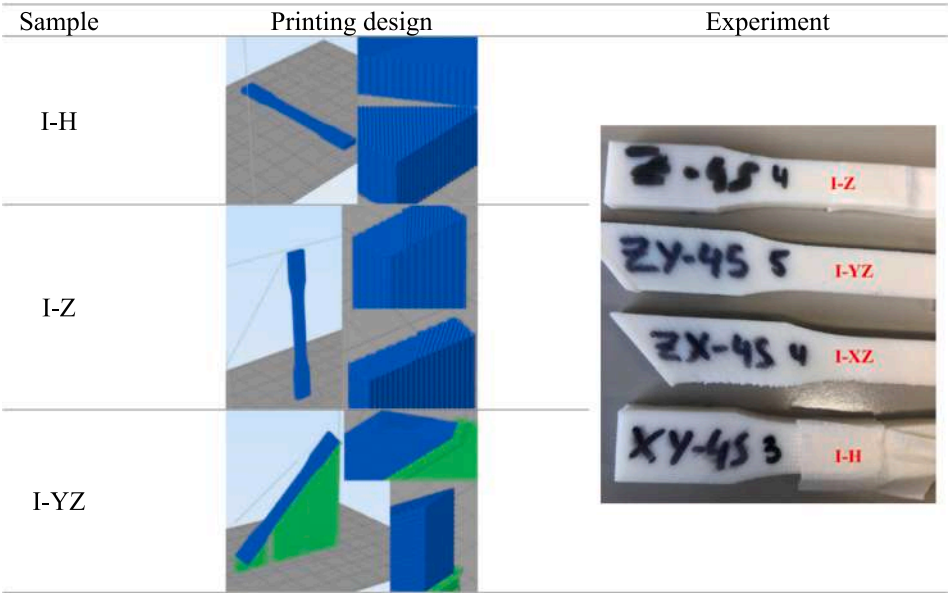

Fig. 9. I samples (cover): Printing design and printed specimen.

- Young's modulus in the direction parallel to the filament ($E_{||}$).
- Young's modulus in the direction perpendicular to the filament and in the plane of isotropy (E_{iso}).
- Poisson's ratio of the plane of isotropy (ν_{iso}).
- Poisson's ratio in the direction parallel to the filament (ν).
- Shear modulus of the plane of isotropy ($G_{\text{iso}} = E_{\text{iso}}/(2(1+\nu_{\text{iso}}))$).
- Shear modulus in the direction parallel to the filament (G).

Cover:

- Young's modulus in the direction parallel to the printing direction of the specimen and perpendicular to the plane of isotropy ($E_{\perp}$).
- Young's modulus in the printing plane (plane of isotropy) with rectilinear filament pattern (E_{iso}).
- Poisson's ratio of the plane of isotropy (ν_{iso}).
- Poisson's ratio in the printing direction (ν).
- Shear modulus of the plane of isotropy (G_{iso}).
- Shear modulus in the printing direction (G).

According to this nomenclature, the **S**-tensor for the contour, when its isotropy plane is YZ as the filament is deposited in the X direction, reads.

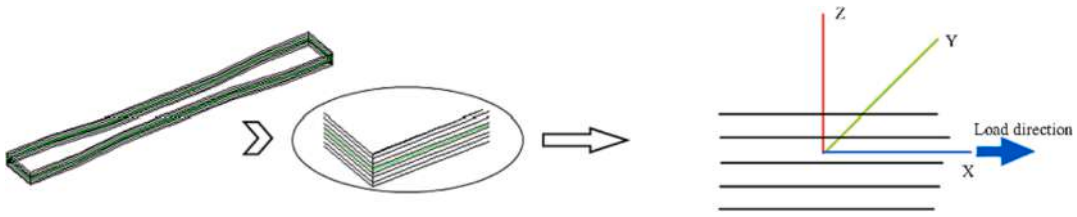

Fig. 10. Obtaining Young's Modulus Parallel to the deposition of the contour material.

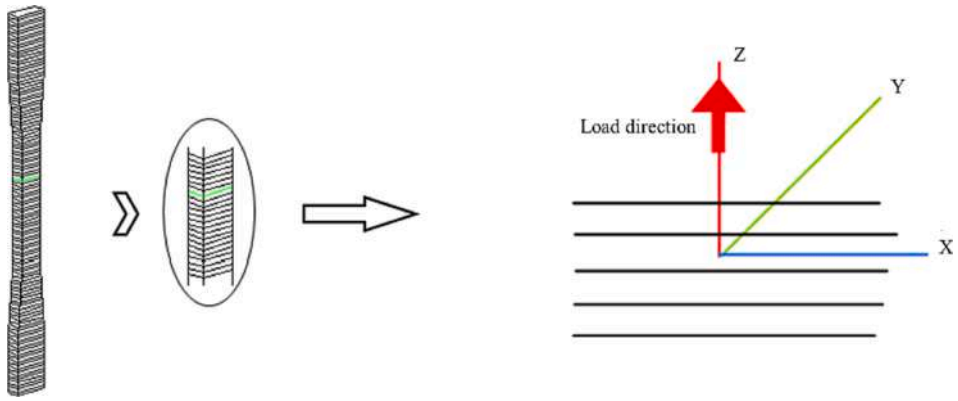

Fig. 11. Obtaining isotropic Young's Modulus for contour material.

$$\mathbf{S} = \begin{bmatrix} \frac{1}{E_{||}} & -\frac{\nu_{iso}}{E_{iso}} & -\frac{\nu}{E_{iso}} & 0 & 0 & 0 \\ -\frac{\nu_{iso}}{E_{iso}} & \frac{1}{E_{iso}} & -\frac{\nu_{iso}}{E_{iso}} & 0 & 0 & 0 \\ -\frac{\nu}{E_{iso}} & -\frac{\nu_{iso}}{E_{iso}} & \frac{1}{E_{iso}} & 0 & 0 & 0 \\ 0 & 0 & 0 & \frac{1}{G} & 0 & 0 \\ 0 & 0 & 0 & 0 & \frac{1}{G} & 0 \\ 0 & 0 & 0 & 0 & 0 & \frac{1}{G_{iso}} \end{bmatrix} \quad (2)$$

Similarly, the **S**-tensor for the cover, where the constructing plane XY is the plane of isotropy, reads.

$$\mathbf{S} = \begin{bmatrix} \frac{1}{E_{iso}} & -\frac{\nu_{iso}}{E_{iso}} & -\frac{\nu}{E_{\perp}} & 0 & 0 & 0 \\ -\frac{\nu_{iso}}{E_{iso}} & \frac{1}{E_{iso}} & -\frac{\nu}{E_{\perp}} & 0 & 0 & 0 \\ -\frac{\nu}{E_{\perp}} & -\frac{\nu}{E_{\perp}} & \frac{1}{E_{\perp}} & 0 & 0 & 0 \\ 0 & 0 & 0 & \frac{1}{G_{iso}} & 0 & 0 \\ 0 & 0 & 0 & 0 & \frac{1}{G} & 0 \\ 0 & 0 & 0 & 0 & 0 & \frac{1}{G} \end{bmatrix} \quad (3)$$

Once the tensors are defined, the parameters are obtained from the experiments.

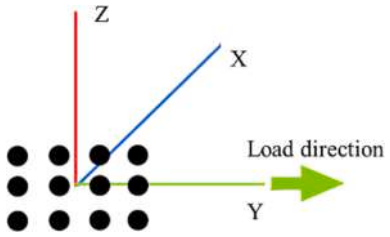

Fig. 12. Scheme of load application to obtain the Poisson's ratio of the isotropy plane for the contour material.

2.1.1.1. Material properties of the contour. Young's modulus in the direction parallel to the filaments ($E_{||}$) is obtained from the horizontally printed P-H specimen. The load is applied in the direction of the filaments. (see Fig. 10).

$$E_{||} = \frac{\sigma_{xx}}{\varepsilon_{xx}} \quad (4)$$

Young's modulus corresponding to the plane of isotropy (E_{iso}) is obtained from the vertically printed specimen P-Z. The load is applied in the direction perpendicular to the filaments (see Fig. 11).

$$E_{iso} = \frac{\sigma_{zz}}{\varepsilon_{zz}} \quad (5)$$

Poisson's ratio ν is obtained by performing a DIC test on the P-Z specimens. The force is applied perpendicular to the direction of the filament and the deformation is measured in the direction perpendicular and parallel to the filament.

To obtain Poisson's ratio ν_{iso}, a specimen should be tested with the applied force in one of the isotropic axes (Fig. 12) in the plane of filaments cross-section. The deformation is measured in both isotropic axes. In this case, the isotropic Poisson's ratio is equal to the anisotropic Poisson's ratio. Alternatively, $\nu_{iso} = \nu$ can be assumed.

The shear modulus G is obtained from uniaxial tensile test of specimen printed in 45°, in this case P-YZ.

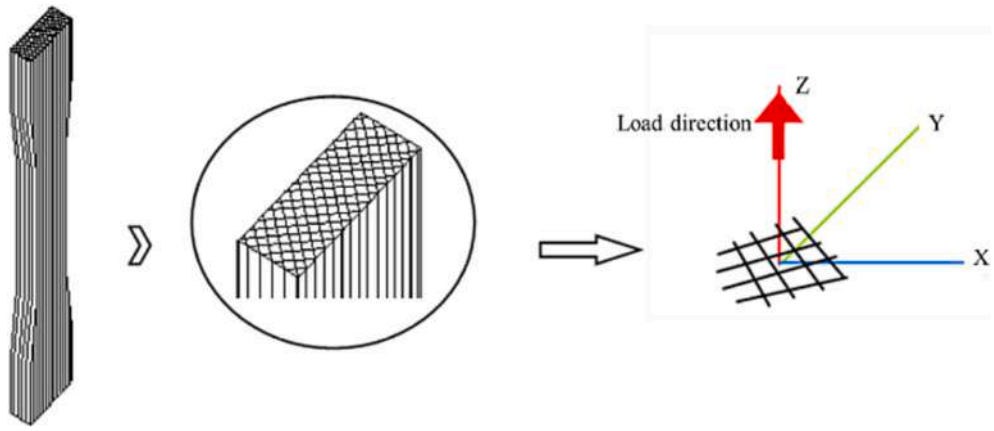

Fig. 13. Obtaining Young's modulus in the construction direction for the cover material.

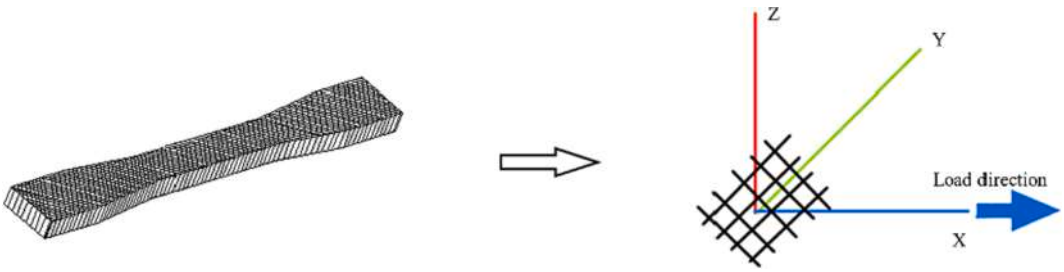

Fig. 14. Obtaining isotropic Young's Modulus for the cover material.

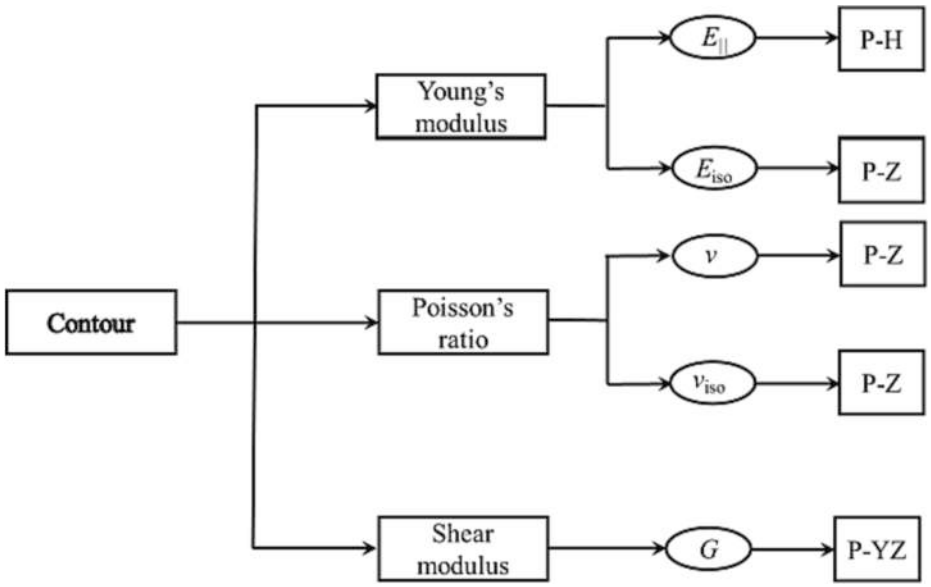

Fig. 15. Diagram for obtaining the parameters from the tests (contour material).

$$G = \left.\frac{E_1}{2(1+\nu_{12})}\right|_{YZ} \tag{6}$$

where 1 is the direction of the applied load and 2 is the direction perpendicular to 1.

2.1.1.2. Material properties of the cover. Young's modulus in the direction parallel to the construction direction ($E_{\perp}$) is obtained from the I-Z specimen. The load is applied in the construction direction. (see Fig. 13).

$$E_{\perp} = \frac{\sigma_{zz}}{\varepsilon_{zz}} \tag{7}$$

E_{iso} is the elasticity modulus obtained from carrying out a tensile test in the isotropic plane. The tensile force is applied in one of the isotropic directions and its corresponding modulus is measured. In this case I-H specimens are used (see Fig. 14).

$$E_{iso} = \frac{\sigma_{xx}}{\varepsilon_{xx}} \tag{8}$$

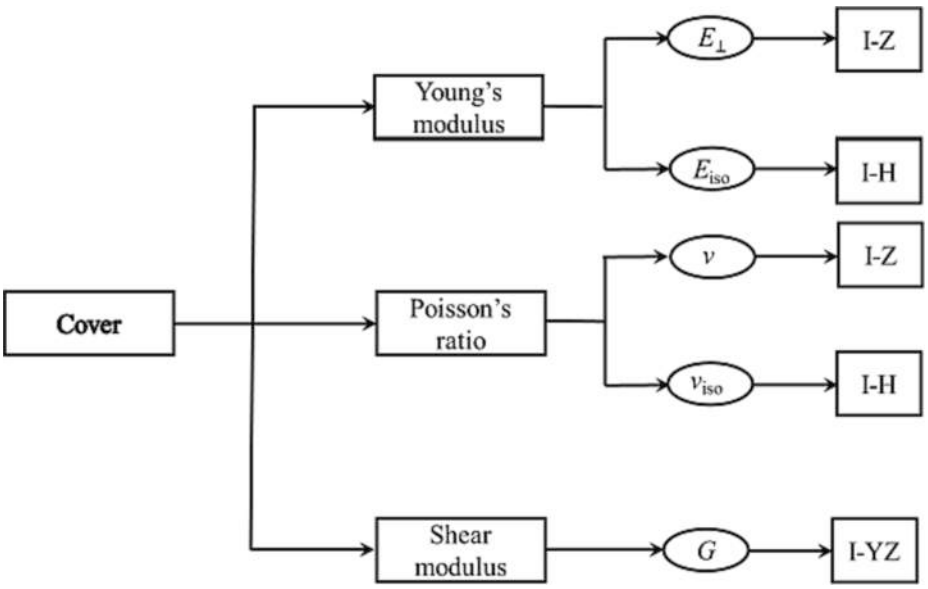

Fig. 16. Diagram for obtaining the parameters from the tests (cover material).

Table 4
Material properties of contour and cover.

Material properties		Contour	Cover
$E_{\|\|}$ (GPa)	$E_\perp$ (GPa)	1.94	0.90
E_{iso} (GPa)		1.59	1.54
ν_{iso}		0.30	0.33
ν		0.30	0.33
G (GPa)		0.60	0.45

Poisson's ratio ν is obtained by performing a DIC test on I-Z specimens since a force is applied perpendicular to the direction of the filament. The deformation is measured in the direction perpendicular and parallel to the filament. However, a Poisson's ratio equal to that in the plane of isotropy is assumed as it has not been possible to obtain this value from experimental tests.

To obtain Poisson's ratio ν_{iso}, a DIC test on the I-H specimen is performed. The force is applied in one of the isotropic axes and the deformation is measured in both isotropic axes.

G_{iso} is known through the relationship with E_{iso} and ν_{iso}. However, the shear modulus G is obtained from a uniaxial tensile test of a specimen printed in 45°, in this case I-YZ.

Figs. 15 and 16 summarize how each parameter is obtained from the dog-bone specimens uniaxial tests to characterize the material properties of contour and cover, respectively.

From the experimental results and the above mentioned strategy, the transversely isotropic properties of the contour and cover are obtained and presented in Table 4.

The specimens printed with aligned filaments (contour) show a distinct mechanical response from those made by 100 % crossed filaments (cover) and from the raw material. Young's moduli of contour and cover are around 10 % ($E_{||,\ contour}$) to 30 % ($E_{iso,\ contour}$) and 30 % ($E_{iso,\ cover}$) to 60 % ($E_{\perp,\ cover}$) lower than that of the raw material, respectively. These differences are due to the effect of the printing pattern as well as the influence of the intra/inter-layer bonds that play a crucial role in FFF components.

Moreover, it can be seen that the fabricated specimens with aligned filaments are stiffer than those made of crossed filaments acting as a reinforcement in the direction of fibers. Therefore, the proposal to distinguish between the material properties of the contour and the cover in order to analyse the performance of FFF components is experimentally justified.

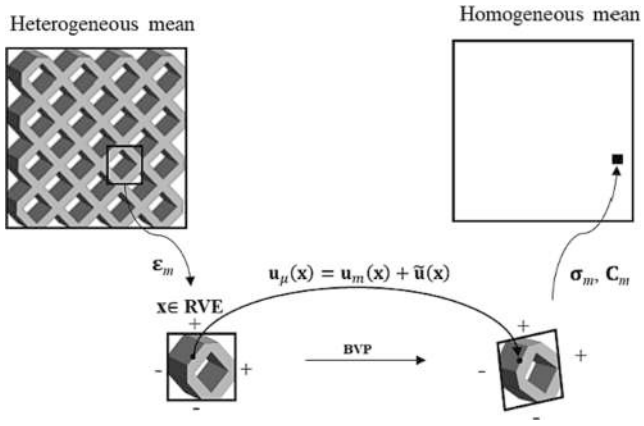

Fig. 17. Homogenization strategy and PBC on the boundary of RVE.

From the experimental results, following relationship between the properties of the isotropic raw material and the printed ones is derived:

- $E_{||,\ contour} \approx 87\ \%\ E_{Raw}$
- $G_{iso,\ contour} \approx 74\ \%\ G_{Raw}$
- $E_{iso,\ contour} \approx 82\ \%\ E_{||,\ contour}$
- $E_{iso,\ cover} \approx 79\ \%\ E_{||,\ contour}$
- $E_{\perp,\ cover} \approx 58\ \%\ E_{iso,\ contour}$

These relationships can be considered for the analysis of FFF components when the experimental campaign for the material characterization according to the printing pattern is to be avoided.

2.2. Computational characterization of the in-fill

Representing the shape details of the heterogeneous in-fill structure within the geometrical model would result in an excessive computational cost of the corresponding simulation (Fig. 1). Therefore, instead of including these details explicitly, a computational homogenization technique is used here. The in-fill structure is modelled as a homogeneous medium with an equivalent constitutive behaviour [28]. It is convenient to use RVE-based homogenization [29–31] since the heterogeneities in the in-fill present periodicity over the domain and the

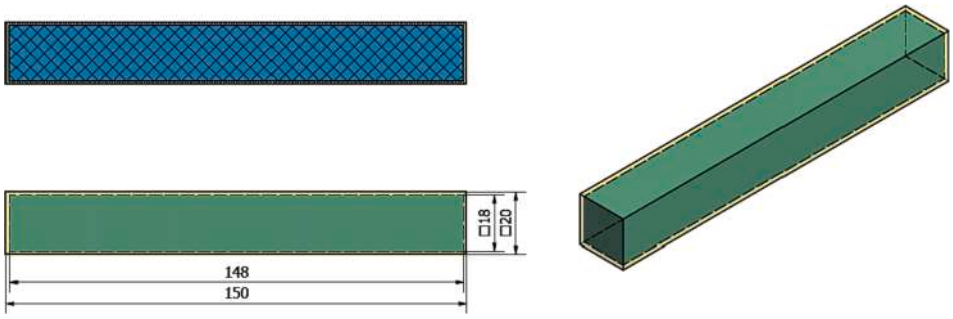

Fig. 18. Geometry of square cross-section demonstrator (dimensions in mm).

structure is characterized by the repetition of a unit cell [32–34].

According to this homogenization technique, the analysis involves two levels: global (macro) and local (micro) with a weak coupling between the two length scales (Fig. 17). The macro and the micro scales conform to the FFF component and the inner structure, respectively.

The displacement field in the macro scale $\mathbf{u}_m(\mathbf{X})$ is assumed to be linear in terms of the spatial coordinate $\mathbf{X}$ of the macro scale. Thus, the macroscopic strains $\varepsilon_m(\mathbf{X}) = \nabla^S \mathbf{u}_m(\mathbf{X})$ are constant.

The solution space $\mathbf{u}_\mu(\mathbf{x})$ defined at each point $\mathbf{x}$ of the micro scale is enriched by a fine scale contribution $\widetilde{\mathbf{u}}(\mathbf{x})$; so that.

$$\mathbf{u}_\mu(\mathbf{x}) = \mathbf{u}_m(\mathbf{x}) + \widetilde{\mathbf{u}}(\mathbf{x}) \tag{9}$$

According to the computational homogenization technique [35] and following the steps described in [32–34], the homogenization procedure consists of:

- **Down-scaling.**

The *constant* macroscopic strains $\boldsymbol{\varepsilon}_m$, are passed from the macro scale to the micro scale as input for solving the micro scale boundary value problem (BVP) on the RVE.

A matrix $\mathbf{E}$ is made of the components of the global strains, $\boldsymbol{\varepsilon}_m^{(i)}$, $i = [1,6]$ (3 elongations and 3 distortions), as:

$$\mathbf{E} = \begin{bmatrix} \boldsymbol{\varepsilon}_m^{(1)} & \cdots & \boldsymbol{\varepsilon}_m^{(6)} \end{bmatrix} = \begin{bmatrix} \varepsilon_{m,x}^{(1)} & \cdots & \varepsilon_{m,x}^{(6)} \\ \vdots & \ddots & \vdots \\ \varepsilon_{m,yz}^{(1)} & \cdots & \varepsilon_{m,yz}^{(6)} \end{bmatrix} \tag{10}$$

- **Solution of the RVE problem.**

A BVP is solved in the RVE domain. The BVP defines the equilibrium of the RVE as.

$$\int_{V_{RVE}} \nabla^S \widetilde{\mathbf{v}}(\mathbf{x}) \sigma_\mu(\mathbf{x}) dV = 0 \tag{11}$$

by applying the Galerkin approach at the level of the fine scale (RVE). Functions $\widetilde{\mathbf{v}}$ correspond to the Finite Element discretization of the RVE.

At the micro scale, the stress–strain relationship is.

$$\boldsymbol{\sigma}_\mu(\mathbf{x}) = \mathbf{C}_\mu(\mathbf{x})\boldsymbol{\varepsilon}_\mu(\mathbf{x}) = \mathbf{C}_\mu(\mathbf{x})\big(\boldsymbol{\varepsilon}_m(\mathbf{X}) + \nabla^S \widetilde{\mathbf{u}}(\mathbf{x})\big) \tag{12}$$

where $\boldsymbol{\sigma}_\mu$ is the microscopic stress field at each point $\mathbf{x}$ of the computational domain, $\mathbf{C}_\mu$ the microscopic constitutive tensor and $\boldsymbol{\varepsilon}_\mu$ microscopic strains.

The RVE problem is solved with the corresponding boundary conditions. In this work, Periodic Boundary Conditions (PBC) are applied to the RVE models as the inner structure can be represented by a periodical array of the RVEs. This means that.

$$\widetilde{\mathbf{u}}(\mathbf{x}^+) = \widetilde{\mathbf{u}}(\mathbf{x}^-) \forall \{\mathbf{x}^+, \mathbf{x}^-\} \in \Gamma_{RVE} \tag{13}$$

where $\mathbf{x}^+ \in \Gamma_{RVE}^+$ and $\mathbf{x}^- \in \Gamma_{RVE}^-$ are all pairs of points belonging to the opposite surfaces of the RVE boundary $\Gamma_{RVE} = \Gamma_{RVE}^+ \cup \Gamma_{RVE}^-$.

Moreover, the traction continuity condition for a periodic RVE model is (Xia el al, 2003 [36]).

$$\mathbf{t}_\mu(\mathbf{x}^+) = -\mathbf{t}_\mu(\mathbf{x}^-) \forall \{\mathbf{x}^+, \mathbf{x}^-\} \in \Gamma_{RVE} \tag{14}$$

- **Up-scaling.**

The solution obtained at local level is returned to the macro scale through the homogenization process over the RVE. Using averaging equations, the homogenized macroscopic stress tensor is derived. The relationship between the local stresses $\boldsymbol{\sigma}_\mu$ and global stresses $\boldsymbol{\sigma}_m$ is defined by integrating over the RVE volume V_{RVE}.

$$\boldsymbol{\sigma}_m(\mathbf{X}) = \frac{1}{V_{RVE}} \int_{V_{RVE}} \boldsymbol{\sigma}_\mu(\mathbf{x}) dV \tag{15}$$

The elastic constitutive relation of the material for a homogenized RVE is given as.

$$\boldsymbol{\sigma}_m(\mathbf{X}) = \mathbf{C}_m(\mathbf{X})\boldsymbol{\varepsilon}_m(\mathbf{X}) \tag{16}$$

$$\begin{bmatrix} \boldsymbol{\sigma}_m^{(1)} & \cdots & \boldsymbol{\sigma}_m^{(6)} \end{bmatrix} = \mathbf{C}_m(\mathbf{X}) \begin{bmatrix} \boldsymbol{\varepsilon}_m^{(1)} & \cdots & \boldsymbol{\varepsilon}_m^{(6)} \end{bmatrix}$$

where $\mathbf{C}_m$ is the effective constitutive matrix of the anisotropic material. Thus.

$$\mathbf{C}_m = \mathbf{S}\mathbf{E}^{-1} \tag{17}$$

where $\mathbf{S}$ is a matrix with columns made of global stresses vector $\boldsymbol{\sigma}_m^{(i)}$, after solving the i^{th} BVP, $i = [1,6]$. Thus:

$$\mathbf{S} = \begin{bmatrix} \boldsymbol{\sigma}_m^{(1)} & \cdots & \boldsymbol{\sigma}_m^{(6)} \end{bmatrix} = \begin{bmatrix} \sigma_{m,x}^{(1)} & \cdots & \sigma_{m,x}^{(6)} \\ \vdots & \ddots & \vdots \\ \sigma_{m,yz}^{(1)} & \cdots & \sigma_{m,yz}^{(6)} \end{bmatrix} \tag{18}$$

3. Validation: Test on samples with square cross-section

The proposed model for the performance analysis of FFF components through separating the mechanical behaviour of the contour, the cover and the in-fill is now validated.

In this section, the validation procedure includes the experimental determination of the respective material properties of the contour and the cover and the computational characterization of the in-fill material. For this reason, samples with square cross-section subjected to bending load are designed and printed. Additionally, the effect of the printing orientation and raster to raster air gap on the final structural behaviour is studied.

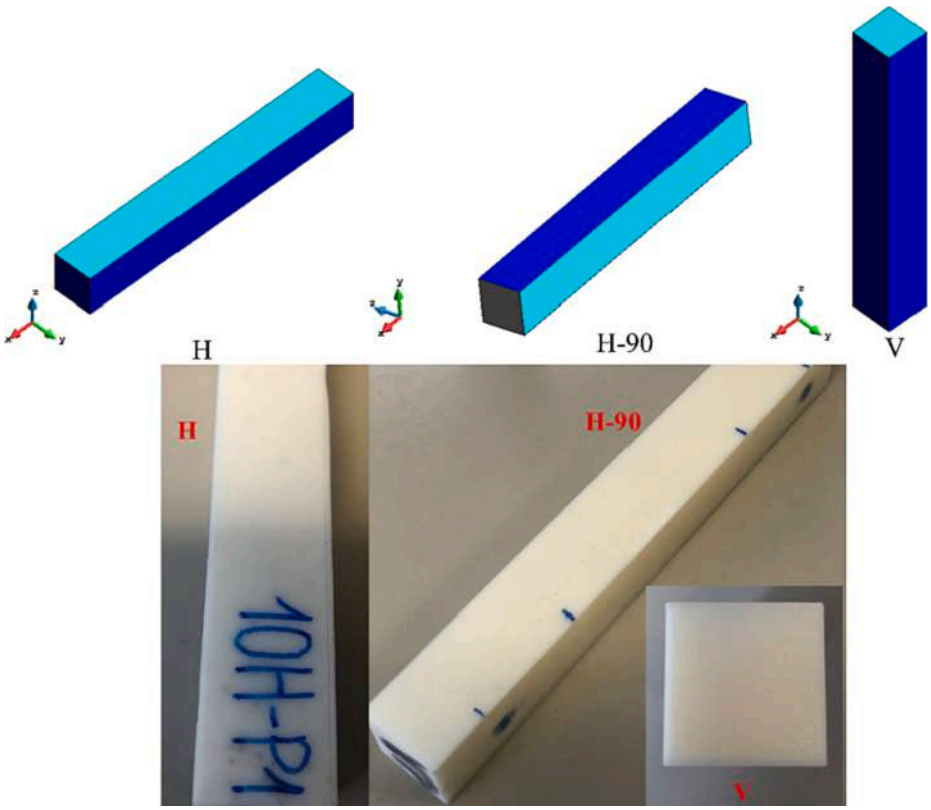

Fig. 19. Samples with square cross-section printed at different orientations: H, H-90 and V.

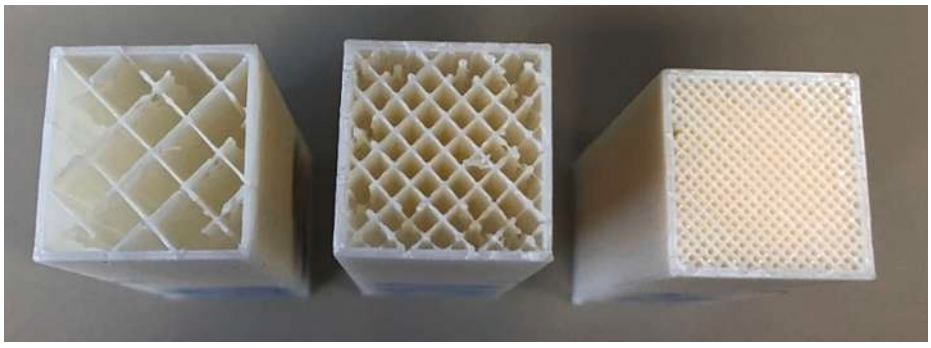

Fig. 20. Cross-section of a broken V sample with 10%, 20% and 60% in-fill density (left to right).

3.1. Experimental validation

These tests are performed in accordance with the ASTM 790 standard test methods for flexural properties of unreinforced and reinforced plastics and electrical insulating materials.

The components are built with a cross-section of 20 mm in width and 20 mm in depth (Fig. 18). The total length of the specimens is 150 mm, with a span between supports of 120 mm.

The contour and the cover have 1 mm thickness (Fig. 18). The in-fill volume indicated with green colour is printed with a 45° rectilinear pattern and the specified density. The in-fill printing pattern is shown in blue.

Forty-five FFF samples of ELIX ABS-3D GP material are produced with different in-fill densities (10 %, 20 % and 60 %) and printing orientations:

- H samples are manufactured horizontally and supported in the building face.
- H-90 samples are manufactured horizontally and supported perpendicular to the building face.
- V Samples are manufactured vertically.

Fig. 19 shows the printed samples at different orientations. A cross section of the V sample with 10 %, 20 % and 60 % in-fill densities is shown in Fig. 20.

A displacement rate of 1.2 mm/min for load application is selected. The yield point is evaluated following the offset method for determining yield strength with an offset value of 0.1 %. The experimental setup is shown in Fig. 21 for sample H with 10 % in-fill density.

The corresponding stress–strain relationship for each specimen obtained from the test is presented in Table 5. The stiffness, maximum load and material failure depending on the printing and testing direction alter. They show that the mechanical behaviour of the printed samples are different depending on the in-fill density and the printing orientation.

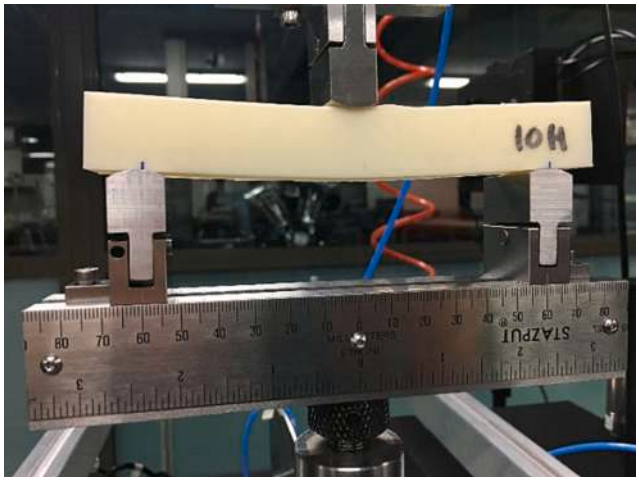

Fig. 21. Experimental setting and the load position (square cross-section demonstrator).

Table 5
Average stress and average strain: Flexural test on square cross-section samples.

	σ_M	ε_M		σ_M	ε_M
	MPa	%		MPa	%
10H-C1	10.0753595	3.51371139	**20H-*P3***	11.6289246	2.70374667
10H-C2	11.7421915	2.84862737	**20H-*P4***	13.6739106	3.39776449
10H-C3	13.0198936	3.27642461	**20H-P5**	9.97002034	2.32451269
10H-C4	13.4260942	3.66691239	**20Z-1**	10.5671288	2.25037934
10H-C5	13.2135325	3.29637197	**20Z-2**	8.71434028	1.73762198
10H-P1	10.347291	3.23072936	**20Z-3**	9.14848721	1.80013262
10H-P2	11.4681991	2.9329961	**20Z-4**	7.97859091	1.64170681
10H-P3	11.0421912	2.68966047	**20Z-5**	10.3155669	2.06372299
10H-P4	11.0946211	2.83937364	**50H-C1**	19.3737095	4.5226658
10H-P5	11.5323543	2.83305209	**50H-C2**	20.2738211	4.61885449
10Z-1	8.06595335	1.83794604	**50H-C3**	19.7236638	3.8543269
10Z-2	7.61100739	1.8085236	**50H-C4**	20.4931086	4.70591878
10Z-3	5.71656406	1.37762926	**50H-C5**	22.0102424	4.71601624
10Z-4	6.66029686	1.50435025	**50H-*P1***	20.1164082	4.15440394
10Z-5	6.60060554	1.4396279	**50H-*P2***	18.8459642	3.56691737
20H-C1	14.2300902	3.25899609	**50H-*P3***	18.5450687	3.26848262
20H-C2	14.6016528	3.66270432	**50H-*P4***	21.6643597	4.36159306
20H-C3	12.5408155	2.97008951	**50H-P5**	17.5566543	2.9687565
20H-C4	11.7096547	3.40082851	**50Z-1**	12.7314719	1.7039615
20H-C5	14.698089	3.68214768	**50Z-2**	12.7453571	1.73168008
20H-P1	11.702998	2.69142189	**50Z-3**	13.9949022	2.00365043
20H-P2	8.84606919	2.08834727	**50Z-4**	14.0238188	1.96396175
			50Z-5	6.87612213	0.95203708

Table 6
In-fill material properties (square cross-section sample).

%In-fill		**10 %**	**20 %**	**60 %**
Young's modulus (MPa)	E_x	0.61	5.50	263.45
	E_y	0.61	5.50	263.45
	E_z	194.00	388.00	1164.00
Shear modulus (MPa)	G_{xy}	53.83	108.62	347.75
	G_{yz}	38.91	81.23	305.80
	G_{xz}	38.91	81.23	305.80
Poisson's ratio	ν_{xy}	0.9940	0.9747	0.7015
	ν_{yz}	0.2992	0.3000	0.3000
	ν_{xz}	0.3007	0.3000	0.3000

Table 7
Mechanical response of the square cross-section sample and the relative error according to each orientation and printing parameters.

In-fill density	Specimen type	$K_{experimental}$ (N/mm)	Displacement (mm)	$K_{simulation}$ (N/mm)	Relative error %
10	H	179.91	1.801	166.55	7
	H-90	166.02	1.859	161.36	3
	V	171.11	1.990	150.76	12
20	H	193.77	1.636	183.38	5
	H-90	188.43	1.644	182.46	3
	V	197.78	1.467	204.55	3
50	H	257.46	1.175	255.22	1
	H-90	274.10	1.128	265.94	3
	V	280.87	1.122	267.38	5

3.2. Computational modeling

In the computational modelling, the geometry manufactured in a 3D printer with FFF technique is split into three regions corresponding to each printing pattern.

The simulation is performed under the same condition as the experiment. The numerical model combines the use of the several software modules. Kratos [37], an in-house multi-physics software, characterizes the in-fill structures by homogenization techniques via RVE with application of PBC. The RVE of the inner structure is shown in Fig. 17. Comet [38], an in-house software, analyses the overall structural behaviour of FFF built components using the material constitutive tensors obtained from Kratos (the inner structure) and the experimental tests on dog-bone samples (the contour and cover).

The material properties of cover and contour characterized in the previous section are assigned to the corresponding volumes. The material properties of the in-fill obtained by the computational homogenization technique is shown in Table 6. The mechanical properties of the in-fill reflect the percentage of air gap between the filaments as well as their orientations.

For each configuration, defined according to the printing design parameters, Table 7 presents the relative error between the stiffness obtained from the experimental tests K_{exp} and the one obtained from the mechanical simulation K_{sim}. The experimental stiffness is obtained through the linear relationship between the applied displacement and the resulting force. The computational stiffness is obtained through the same linear relationship between the applied force and the resulting displacement. Remarkably, the relative error in the majority of the cases is less than 5 %.

Moreover, Fig. 22 compares the numerical and the experimental force vs displacement graphs for all the combination of in-fill densities. The agreement between the numerical and experimental results is noteworthy.

From this, it is concluded that characterizing the material behaviour of the component according to the printing pattern is necessary for the correct prediction of the mechanical performance. Moreover, the transversely isotropic description of the contour and the cover materials plus the use of homogenization technique for characterization of the in-fill material represent accurately the behaviour of the samples.

From the results of the tests on samples with positions H and H-90, the differences between the mechanical behaviour of the cover and the contour can be understood. These results show that the same printed component presents different mechanical response if the load is applied on the cover (in case of H samples) or on the contour (in case of H-90 samples). Moreover, the mechanical performance of these samples is affected by the in-fill density and orientation.

Increasing the in-fill density increases the stiffness of the structure. In particular, the vertically printed samples (V specimens) are the most influenced by the increment of the in-fill density. V specimens include more contour area than cover than the other two cases and the contour material is stiffer than the cover.

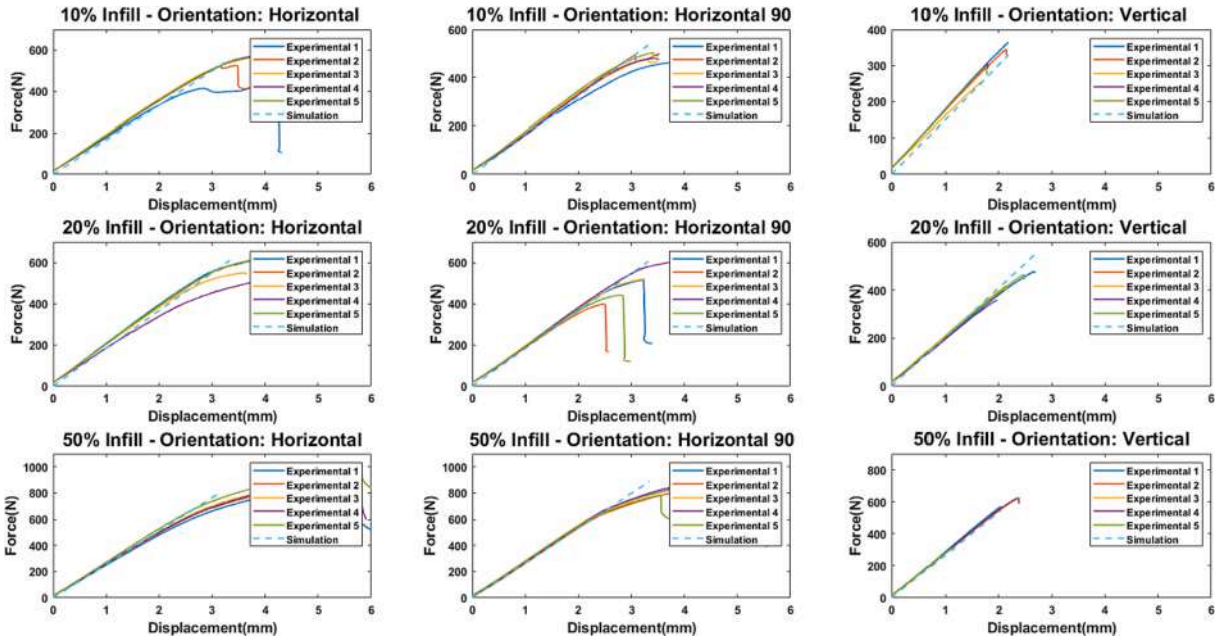

Fig. 22. Force (N) vs displacement (mm) curves comparing the simulation results with the experimental measurements.

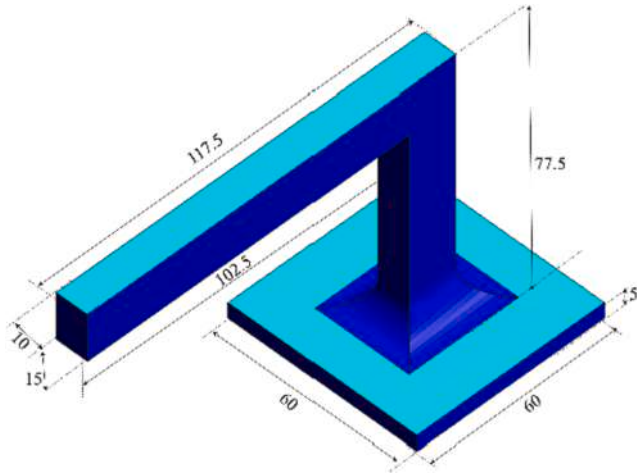

Fig. 23. Door-handle dimension (mm): cover (light blue) and contour (dark blue).

4. Validation: door-handle under bending and torsion

In this section, the proposed model for the performance analysis of FFF components is validated when the experimental data to obtain the mechanical properties of the contour and the cover is unavailable. The material behaviour of the contour and cover can be characterized by an anisotropic constitutive relationship based on the printing patterns as a function of raw material or filament properties.

For this reason, the door-handle components are printed with a material different than ABS-3D GP and tested to validate these geometrical relationships. The mechanical performance of these pieces is analysed at different printing orientations, in-fill density and contour thickness.

4.1. Experimental validation

The filament material for manufacturing the door-handle components is PLA extruded at 215 °C. The door-handle dimensions are shown in Fig. 23. The printer is Original Prusa i3 MK2S. Three printing orientations are considered as shown in Fig. 24. Light and dark blue colours stand for the cover and the contour in each orientation being parallel and perpendicular to the printing plane, respectively.

Four combinations of two in-fill densities (25 % and 50 %) and two contour types (single or double contour thickness) are considered to investigate the effect of the printing parameters. The in-fill pattern is rectilinear with 45° raster angle.

A vertical displacement of 35 mm, 15 mm away from the end of the component is applied with a speed of 1 mm/min (Fig. 25). In this way, the door-handle is subjected to a combination of bending and torsion resulting in a complex stress state. The force results from the vertical downward displacement of the force applicator, which moves at 1 mm/min. The stiffness is obtained from the linear relationship between the force and the displacement.

4.2. Computational modeling

As proposed in this work, the volume of the component is divided into three computational zones distinguishing between the contour, the cover and the in-fill.

Since the characterization of the anisotropic material of each zone is a complex task and requires an extensive experimental campaign, linear proportionality between the mechanical properties and the degree of anisotropy due to the printing pattern is assumed as explained and justified in section 2.1. In this way, knowing only two isotropic mechanical properties of the material, the rest of properties can be defined. This is in particular advantageous when the material properties of the contour and cover are not known and the only available data is the isotropic raw material properties.

Initially, these parameters are defined through the relationship obtained in the case of ABS-3D GP with the raw material properties:

- $E_{||,\ \mathrm{contour}} \approx 87\ \%\ E_{\mathrm{Raw}}$
- $G_{\mathrm{iso},\ \mathrm{contour}} \approx 74\ \%\ G_{\mathrm{Raw}}$

Once $E_{||,\ \mathrm{contour}}$ and $G_{\mathrm{iso},\ \mathrm{contour}}$ are known the rest of the material properties for both contour and cover are found.

- $E_{\mathrm{iso},\ \mathrm{contour}} \approx 82\ \%\ E_{||,\ \mathrm{contour}}$
- $E_{\mathrm{iso},\ \mathrm{cover}} \approx 79\ \%\ E_{||,\ \mathrm{contour}}$

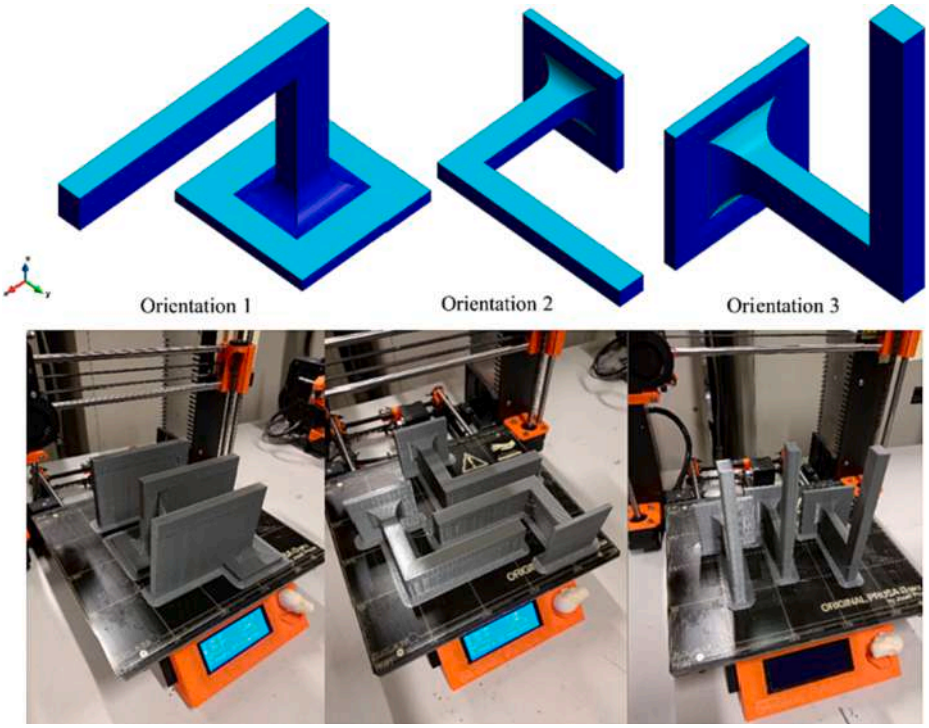

Fig. 24. Door-handle printing orientations: cover (light blue) and contour (dark blue).

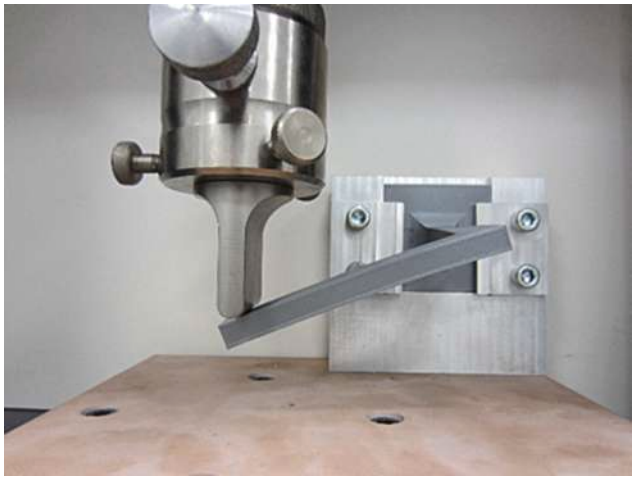

Fig. 25. Experimental setting and the load position.

- $E_{\perp,\ \text{cover}} \approx 58\ \%\ E_{\text{iso,\ contour}}$.

The raw material properties are defined by the manufacturer: Young's modulus (E_{Raw}) = 3368 MPa and Poisson's ratio (ν_{Raw}) = 0.35 [39].

The computational modelling is performed using the software modules: Kratos, Comet and Dakota.

The initial data of the calibration loop is the raw material properties. Dakota [40], an optimization software developed by Sandia National Labs, minimizes the difference between the structural stiffness resulted from the experimental data K_{exp} and the numerical analysis K_{sim} using Comet. This is an iterative procedure in order to find the optimal material parameters. Coliny *derivative-free* method is selected to minimize the objective function, S defined as:

Table 8
Optimal material properties of contour and cover (door-handle).

Material properties		Contour	Cover
$E_{\|\|}$ (GPa)	$E_{\perp}$ (GPa)	3.05	1.415
E_{iso} (GPa)		2.5	2.421
ν_{iso}		0.24	0.24
ν		0.24	0.24
G (GPa)		0.943	1.21

Table 9
Material properties of in-fill (door-handle).

%In-fill		**25 %**	**50 %**
Young's modulus (MPa)	E_x	17.41	201.65
	E_y	17.41	201.59
	E_z	762.45	1525.0
Shear modulus (MPa)	G_{xy}	210.30	444.00
	G_{yz}	171.26	392.84
	G_{xz}	171.26	392.84
Poisson's ratio	ν_{xy}	0.96	0.81
	ν_{yz}	0.24	0.24
	ν_{xz}	0.24	0.24

$$S = \sum_{i=1}^{n} r_i^2, \tag{19}$$

Where $r_i = K_{exp,i} - K_{sim,i}$, are the residual errors for each configuration (i) according to the printing design parameters.

The optimized anisotropic material properties of each part in case of PLA filaments are shown in Tables 8 and 9.

From the optimal material properties, it can be deduced that in case of PLA.

- $E_{||,\ \text{contour}} \approx 91\ \%\ E_{\text{Raw}}$

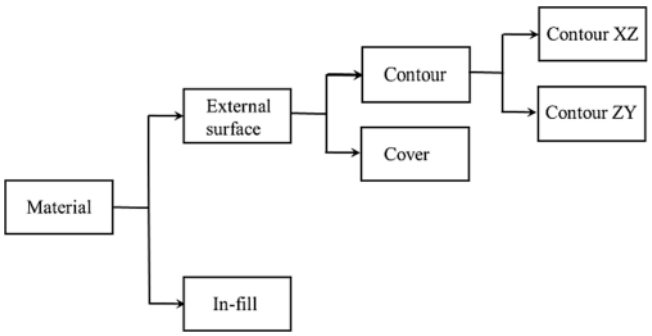

Fig. 26. Materials considered in the simulation of door-handle.

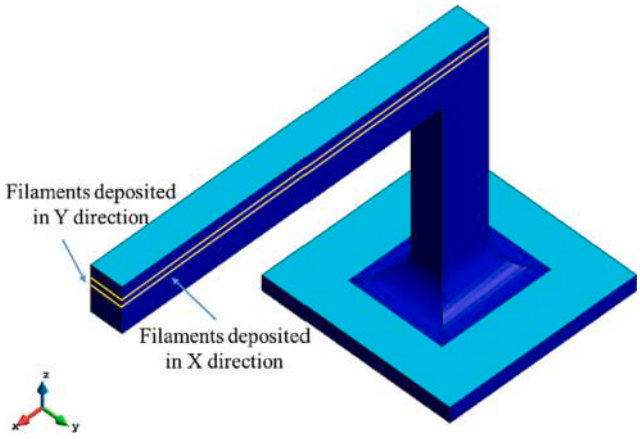

Fig. 27. Different filaments deposition direction.

- $G_{\text{iso, contour}} \approx 81\ \%\ G_{\text{Raw}}$.

The optimal relationship between the input data and the contour properties in the case of PLA is in fair accordance with that of the ABS-3D GP case, taking into account that the material properties defined by each manufacturer can be slightly different.

The validation performed shows that the geometrical relationship can hold for any thermoplastic materials used in FFF avoiding the experimental material characterization of the contour and the cover.

Fig. 26 shows the scheme of the different materials considered in the simulation. Note that the mechanical behaviour of the contour depends on the deposition direction. In the contour, the filament direction is normal to the isotropic plane. Therefore, in the door-handle two contour materials XZ and ZY are considered as the filament deposition direction varies along X and Y axes. Fig. 27 shows that in the case where the filament deposition direction is the X axis, YZ is the isotropic plane and for the case where the filament deposition direction is Y, the XZ plane is considered as the plane of isotropy. This is reasonable, as the moduli in the filament direction are much stiffer than in the perpendicular plane (filament cross-section).

The isotropic plane of the cover as well as the in-fill is the XY plane and the building direction (Z axis) is the anisotropy axis.

Table 10 presents the relative error between $K_{exp,i}$ and $K_{sim,i}$. For most of the cases, the relative error between the structural stiffness resulted from the experiment and the numerical analysis for each printing orientation, contour thickness and in-fill density is below 5 %. Thus, the numerical model predicts correctly the structural behaviour of the demonstrator.

Force vs displacement curves are obtained for each combination according to the design properties. Figs. 28 and 29 show these results for the door-handles. The obtained simulation results correlates very well with the experimental ones.

The demonstrator with 50 % in-fill and double contour is the stiffest while the one with 25 % in-fill and single contour is the weakest. Among the printing orientations, the demonstrator printed in orientation 2 shows the weakest structural behaviour. This sample is characterized by the largest cover area while the samples printed in the other two orientations contain bigger contour area. This confirms that the stiffness of the cover is different and smaller than the contour.

Additionally, it can be concluded that the structural stiffness is more dependent on the contour size than the in-fill density.

These results confirm that the combination of.

- geometrical relationship between the material properties at different orientation and the raw material,
- material characterization according to the printing patterns,
- computational homogenization technique for obtaining the in-fill structure properties and
- transversely isotropic description of the material behaviour

is a feasible strategy for analysing the mechanical performance of FFF built components.

Table 11 compares the results obtained in this work with the result of the numerical simulation when the external contour of the 3D object is assumed single isotropic material [32]. The methodology proposed in this work reduces very much the amount of the relative error. This shows that the external contour material must be split into the contour and the cover according to the printing pattern. Moreover, describing the external contour material as an anisotropic (rather than isotropic) is advantageous.

5. Summary and conclusions

In this work, a hybrid methodology for the material characterization and mechanical performance of FFF components is proposed. The methodology combines experimental and computational

Table 10
Mechanical response of the door-handle and the relative error according to each orientation and printing parameters.

Orientation	# Filaments	In-fill %	Displacement (mm)	$K_{\text{Numerical}}$ (MPa)	Force (N)	$K_{\text{Experimental}}$ (MPa)	ε_{rel}%	r_i^2
1	4	25	6.14	2.44	15	2.444	0	0
2			7.42	2.02		1.877	8	0.021
3			5.96	2.52		2.534	1	0.0002
1	4	50	5.29	2.84	15	3.001	5	0.0264
2			6.44	2.33		2.432	4	0.0103
3			5.22	2.87		3.013	5	0.0192
1	2	25	8.84	1.70	15	1.600	6	0.0094
2			11.7	1.28		1.109	16	0.0301
3			8.77	1.71		1.643	4	0.0046
1	2	50	7.44	2.02	15	2.133	5	0.0135
2			9.01	1.67		1.675	1	0.0000
3			6.76	2.22		2.266	2	0.0023
								$S = 0.137$

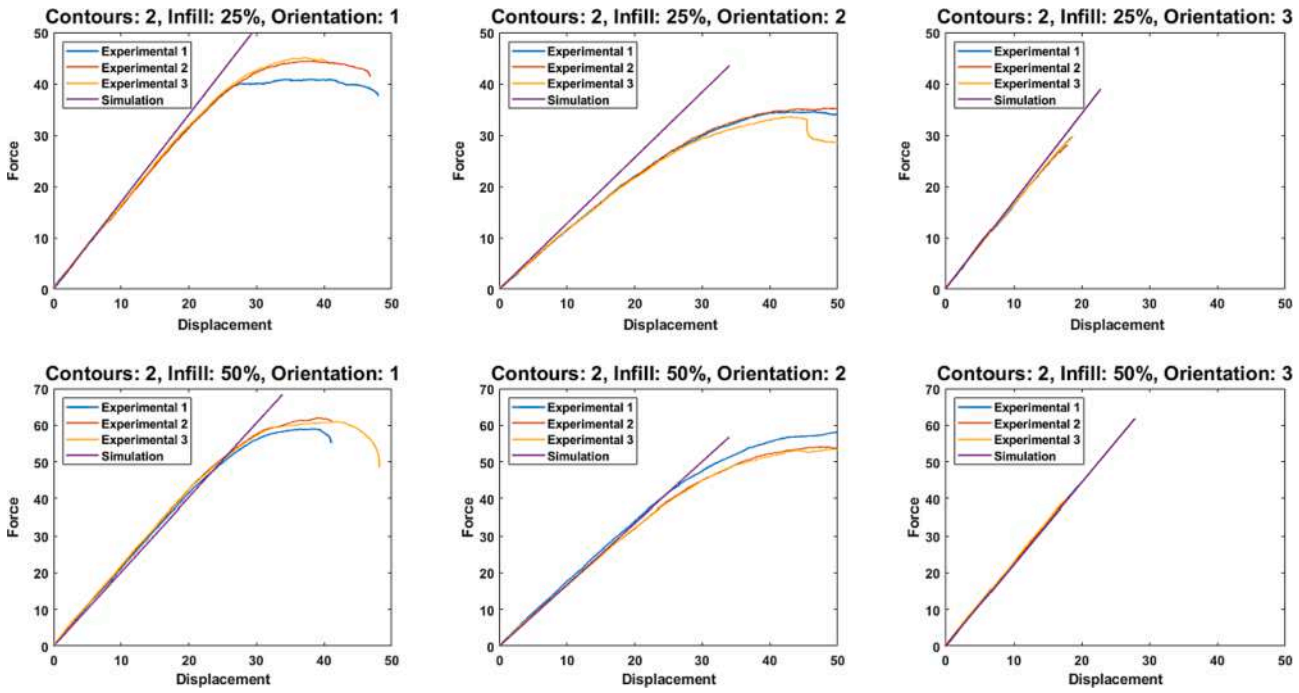

Fig. 28. Force (N) vs displacement (mm) curves comparing the simulation results with the experimental measurements (single contours).

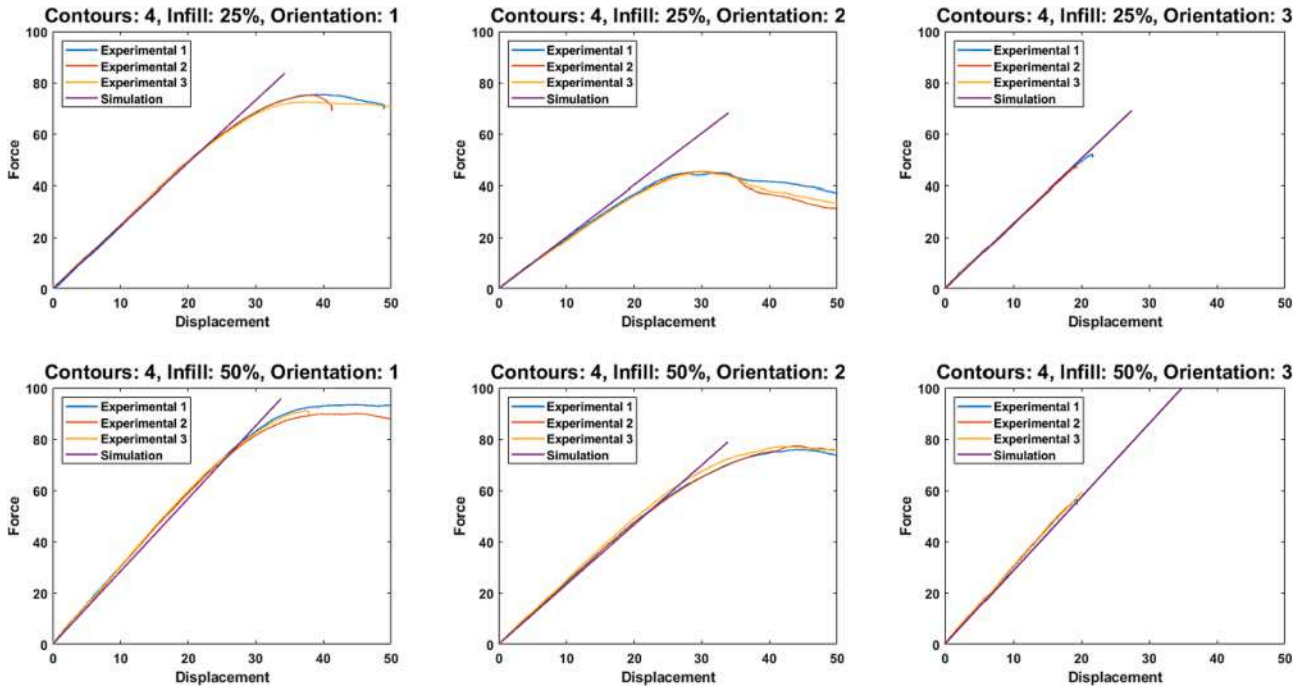

Fig. 29. Force (N) vs displacement (mm) curves comparing the simulation results with the experimental measurements (double contours).

characterization. The mechanical response of the 3D printed structure depends on the printing pattern used for the manufacturing. Accordingly, for performance analysis of the printed structure, the proposed methodology distinguishes between three regions in the FFF component: the contour, the cover and the in-fill structure. The constitutive material characteristic varies depending on the region and exhibit anisotropic behaviour, even though the raw material *per se* is isotropic.

The transversely isotropic material properties of the contour and the cover are characterized through extensive experimental tests performed on the dog-bone FFF specimens. The material characterization is carried out for ELIX ABS-3D GP. It is found that the values of material parameters of contour and cover are different and lower than that of the raw material. To characterize the in-fill material properties, a computational homogenization technique is used with the application of PBC on the chosen RVE. As a result, an equivalent homogeneous but anisotropic constitutive behaviour is obtained.

Square cross-section demonstrators made of ELIX ABS-3D GP are printed using different orientations with a selection of in-fill densities. They are tested experimentally under bending in order to validate the proposal of distinguishing between the mechanical behaviour of the

Table 11
Comparison between the mechanical response of the door-handle considering the external contour as anisotropic contour and cover materials or single isotropic material.

Orientation	# Filaments	In-fill %	$K_{Experimental}$ (MPa)	$K_{Numerical}$ (MPa)	ε_{rel}%	$K_{Numerical}$ (MPa) *Isotropic*	ε_{rel}% *Isotropic*
1	4	25	2.444	2.44	0	2.615	7
2			1.877	2.02	8	2.014	7
3			2.534	2.52	1	2.432	4
1	4	50	3.001	2.84	5	2.819	6
2			2.432	2.33	4	2.319	5
3			3.013	2.87	5	2.773	8
1	2	25	1.600	1.70	6	1.764	10
2			1.109	1.28	16	1.350	22
3			1.643	1.71	4	1.731	5
1	2	50	2.133	2.02	5	2.091	2
2			1.675	1.67	1	1.717	3
3			2.266	2.22	2	2.196	3
					$S = 0.137$		$S = 0.263$

contour, the cover and the in-fill, and the experimental determination of their respective mechanical properties. Increasing the in-fill density increases the stiffness of the component, particularly in the V specimens, and decreases the impact of the in-fill orientation on the final structural behaviour.

A geometrical relationship between the mechanical properties of the raw material and the printed material following the contour and the cover pattern is found. It is shown that the material characterization depends on the geometrical relationship of the different printing patterns, exclusively. Therefore, the exhaustive experimental procedure can be avoided by assuming the printed material can be characterized by a pre-defined anisotropic constitutive relationship (based on printing patterns) and proportional to the material properties of the raw material (i.e. filament properties). This relationship is validated for PLA FFF components. This is especially useful when the properties of the material according to the printing pattern are unknown.

Door-handle demonstrators made of PLA are printed in three different orientations with a selection of in-fill densities and contour thickness. They are tested experimentally under bending and torsion loadings. The effect of the printing orientation and process parameters on the structural stiffness is investigated. It is revealed that the contour thickness influences the component behaviour. The structural stiffness is enhanced by increasing the contour thickness and in-fill density; being the contour thickness more decisive parameter. The printing orientation with the lowest stiffness is found to be the one characterized by the largest cover area.

The satisfactory agreement obtained between the numerical and experimental results confirms that the strategy proposed in this work is capable of predicting the mechanical response of the FFF components. Moreover, it is proved that process parameters such as contour thickness, in-fill density and build orientation play important roles in the mechanical performance of such components.

The model developed in this work is validated for ABS-3D GP samples. The material properties obtained can be used for modelling ABS-3D GP FFF components. In case of raw materials different from those studied in the work there are two possibilities. Either the geometrical relationship obtained can be calibrated as done here for PLA, or, tests and calibration steps can be repeated, for characterization of aligned and crossed filaments of contour and cover, prior to using the model as the predictive tool.

As long as the hypotheses of linear elasticity, small strains and scales separation for the infill structure homogenization hold true, the technique used for numerical simulation of structural behaviour of AM components created by FFF is appropriate.

CRediT authorship contribution statement

Narges Dialami: Conceptualization, Methodology, Validation, Software, Writing – original draft, Writing – review & editing. **Michele Chiumenti:** Conceptualization, Methodology, Software. **Miguel Cervera:** Conceptualization, Methodology, Software, Writing – review & editing. **Uxue Chasco:** Validation, Data curation. **Guillermo Reyes-Pozo:** Data curation. **Marco A. Pérez:** Data curation.

Declaration of Competing Interest

The authors declare that they have no known competing financial interests or personal relationships that could have appeared to influence the work reported in this paper.

Acknowledgments

Narges Dialami is a Serra Húnter Fellow.

This work has been supported by the RIS3CAT Llavor 3D Community co-financed by the Generalitat de Catalunya (ACCIÓ) through the projects TRANSPORT COMRDI16-1-0010 - 00 and PRO2 COMRDI16-1-0009-04.

Financial supports from the European Union's horizon 2020 research and innovation programme (H2020-DT-2019-1 No. 872570) under the KYKLOS 4.0 Project (An Advanced Circular and Agile Manufacturing Ecosystem based on rapid reconfigurable manufacturing process and individualized consumer preferences) and from the Ministry of Science, Innovation and Universities (MCIU) via: the PriMuS project (Printing pattern based and MultiScale enhanced performance analysis of advanced Additive Manufacturing components, ref. num. PID2020-115575RB-I00) are gratefully acknowledged.

The financial support from the Spanish Ministry of Economy and Competitiveness, through the Severo Ochoa Programme for Centres of Excellence in R&D (CEX2018-000797-S), is gratefully acknowledged as well as from CONCYTEC R + D (Project Reference: 163-2017-FONDECYT, in association with Pontifical Catholic University of Perú and CIMNE) -" Optimización del uso de polímeros sintéticos en procesos de manufactura aditiva mediante modelos de simulación computacional y técnicas de caracterización de materiales. Caso de estudio: aplicaciones médicas - prótesis de mano.".

References

[1] Ligon SC, Liska R, Stampfl J, Gurr M, Mülhaupt R. Polymers for 3D Printing and Customized Additive Manufacturing. Chem Rev 2017;117(15):10212–90.
[2] Pîrjan A, Petroşanu D-M. The Impact Of 3d Printing Technology On The Society And Economy. Journal of Information Systems & Operations Management 2013;7 (2):360–70.
[3] Dormehl L. The History of 3D Printing, Told Through 15 Major Milestones. Retrieved October 30, 2018, from Digital Trends website: https://www.digitaltrends.com/cool-tech/history-of-3d-printing-milestones.
[4] Brenken B, Barocio E, Favaloro A, Kunc V, Pipes RB. Fused filament fabrication of fiber-reinforced polymers: A review. Addit Manuf 2018;21:1–16.

[5] Kotlinski J. Mechanical properties of commercial rapid prototyping materials. Rapid Prototyp J 2014;20(6):499–510.
[6] Khudiakova A, Arbeiter F, Spoerk M, Wolfahrt M, Godec D, Pinter G. Inter-layer bonding characterisation between materials with different degrees of stiffness processed by fused filament fabrication. Addit Manuf 2019;28:184–93.
[7] Tao Y, Kong F, Li Z, Zhang J, Zhao X, Yin Q, et al. A review on voids of 3D printed parts by fused filament fabrication. J Mater Res Technol 2021;15:4860–79.
[8] Krajangsawasdi N, Longana ML, Hamerton I, Woods BKS, Ivanov DS. Batch production and fused filament fabrication of highly aligned discontinuous fibre thermoplastic filaments. Additive Manufacturing 2021;48(A):102359.
[9] Di Landro L, Montalto A, Bettini P, Guerra S, Montagnoli F, Rigamonti M. Detection of Voids in Carbon/Epoxy Laminates and Their Influence on Mechanical Properties. Polym Polym Compos 2017;371–380.
[10] Li H, Wang T, Sun J, Yu Z. The effect of process parameters in fused deposition modelling on bonding degree and mechanical properties. Rapid Prototyping Journal 2018;24(1):80–92.
[11] Ding Sh, Zou B, Wang P, Ding H. Effects of nozzle temperature and building orientation on mechanical properties and microstructure of PEEK and PEI printed by 3D-FDM. Polym Test 2019;78:105948.
[12] Chacón JM, Caminero MA, García-Plaza E, Núñez PJ. Additive manufacturing of PLA structures using fused deposition modelling: Effect of process parameters on mechanical properties and their optimal selection. Mater Des 2017;124:143–57.
[13] Zou R, Xia Y, Liu S, Hu P, Hou W, Hu Q, et al. Isotropic and anisotropic elasticity and yielding of 3D printed material. Compos B Eng 2016;99:506–13.
[14] Garzon-Hernandez S, Arias A, Garcia-Gonzalez D. A continuum constitutive model for FDM 3D printed thermoplastics. Compos B Eng 2020;201:108373.
[15] Aloyaydi BA, Sivasankaran S, Ammar HR. Influence of infill density on microstructure and flexural behavior of 3D printed PLA thermoplastic parts processed by fusion deposition modeling. AIMS Mater Sci 2019;6:1033–48.
[16] Ahn S, Montero M, Odell D, Roundy S, Wright PK. Anisotropic material properties of fused deposition modeling ABS. Rapid Prototyping Journal 2002;8(4):248–57.
[17] Somireddy M, Czekanski A. Mechanical Characterization of Additively Manufactured Parts by FE Modeling of Mesostructure. Journal of Manufacturing and Materials Processing 2017;1(2):18.
[18] Dizon JRC, Espera Jr AH, Chen Q, Advincula RC. Mechanical characterization of 3D-printed polymers. Addit Manuf 2018;20:44–67.
[19] Popescu D, Zapciu A, Amza C, Baciu F, Marinescu R. FDM process parameters influence over the mechanical properties of polymer specimens: A review. Polym Test 2018;69:157–66.
[20] Gabor C, Alin MA, Magli D, Bedo T, Munteanu SI, Munteanu D. The optimization of the production procedure in relation to the mechanical properties of additively manufactured parts. Mater Today 2019;19:1008–13.
[21] Domingo-Espin M, Puigoriol-Forcada JM, Garcia-Granada A-A, Llumà J, Borros S, Reyes G. Mechanical property characterization and simulation of fused deposition modeling Polycarbonate parts. Mater Des 2015;83:670–7.
[22] Casavola C, Cazzato A, Moramarco V, Pappalettere C. Orthotropic mechanical properties of fused deposition modelling parts described by classical laminate theory. Mater Des 2016;90:453–8.
[23] Rodríguez JF, Thomas JP, Renaud JE. Mechanical behavior of acrylonitrile butadiene styrene (ABS) fused deposition materials. Experimental investigation Rapid Prototyping Journal 2001;7(3):148–58.
[24] Forés-Garriga A, Pérez MA, Gómez-Gras G, Reyes-Pozo G. Role of infill parameters on the mechanical performance and weight reduction of PEI Ultem processed by FFF. Mater Des 2020;193:108810.
[25] Garg A, Bhattacharya A. An insight to the failure of FDM parts under tensile loading: finite element analysis and experimental study. Int J Mech Sci 2017;120:225–36.
[26] Li L, Sun Q. Composite modeling and analysis for fabrication of FDM prototypes with locally controlled properties. J Manuf Process 2002;4:129–41.
[27] Bellini A, Güçeri S. Mechanical characterization of parts fabricated using fused deposition modeling. Rapid Prototyping Journal 2003;9(4):252–64.
[28] Hill R. Elastic properties of reinforced solids: some theoretical principles. J Mech Phys Solids 1963;5(11):357–72.
[29] Oller S, Miquel Canet J, Zalamea F. Composite material behavior using a homogenization double scale method. J Eng Mech 2005;131(1):65–79.
[30] Otero F, Martínez X, Oller S, Salomón O. Study and prediction of the mechanical performance of a nanotube-reinforced composite. Compos Struct 2012;94:2920–30.
[31] Otero F, Oller S, Martinez X, Salomón O. Numerical homogenization for composite materials analysis. comparison with other micro mechanical formulations. Compos Struct 2015;122:405–16.
[32] Dialami N, Cervera M, Chiumenti M, Rossi R, Chasco U, Domingo M. Numerical and experimental analysis of the structural performance of AM components built by Fused Filament Fabrication. Int J Mech Mater Des 2021;17:225–44. https://doi.org/10.1007/s10999-020-09524-8.
[33] Rivet I, Dialami N, Cervera M, Chiumenti M, Reyes-Pozo G, Pérez MA. Experimental, Computational, and Dimensional Analysis of the Mechanical Performance of Fused Filament Fabrication Parts. Polymers 2021;13:1766.
[34] Dialami N, Rivet I, Cervera M, Chiumenti M. Computational characterization of polymeric materials 3D-printed via fused filament fabrication. Mech Adv Mater Struct 2022;1–11. https://doi.org/10.1080/15376494.2022.2032496.
[35] Suquet P. Local and global aspects in the mathematical theory of plasticity, Plasticity today, 1985: 279–309.
[36] Xia Z, Zhang Y, Ellyin F. A unified periodical boundary conditions for representative volume elements of composites and applications. Int J Solids Struct 2003;40(8):1907–21.
[37] Dadvand P, Rossi R, Oñate E, An object-oriented environment for developing finite element codes for multi-disciplinary applications Archives of computational methods in engineering 2010; 17(3): 253-297.
[38] Cervera M, Agelet de Saracibar C, Chiumenti M. COMET: Coupled Mechanical and Thermal Analysis, Data Input Manual, Version 5. 0, Technical Report IT-308, 2002. <http://www.cimne.upc.es>.
[39] Tymrak BM, Kreiger M, Pearce JM. Mechanical properties of components fabricated with open-source 3-D printers under realistic environmental conditions. Mater Des 2014;58:242–6.
[40] Adams B, Ebeida M, Eldred M, Jakeman J, Swiler L, Bohnhoff W. et al. DAKOTA: a multilevel parallel object-oriented framework for design optimization, parameter estimation, uncertainty quantification, and sensitivity analysis, version 5.3.1 reference manual. Technical Report, U.S. Department of Energy, 2013N.